

DEVELOPMENT OF A CATALYTIC COMBUSTION SYSTEM FOR THE MIT MICRO GAS TURBINE ENGINE

by

Jhongwoo Peck

Bachelor of Science, Mechanical and Aerospace Engineering
Seoul National University, Republic of Korea (August 2001)

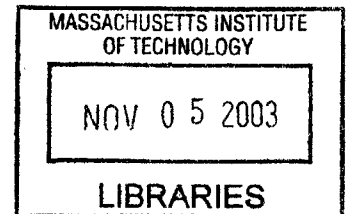
Submitted to the Department of Aeronautics and Astronautics
in partial fulfillment of the requirements for the degree of

Master of Science in Aeronautics and Astronautics

at the

Massachusetts Institute of Technology

September 2003



© 2003 Massachusetts Institute of Technology. All rights reserved.

Author: _____
Jhongwoo Peck
Department of Aeronautics and Astronautics
August 22, 2003

Certified by: _____
Professor and Deputy Head, Department of Aeronautics and Astronautics
Thesis Supervisor
Ian A. Waitz

Accepted by: _____
Edward M. Greitzer
H.N. Slater Professor of Aeronautics and Astronautics
Chair, Committee on Graduate Students

DEVELOPMENT OF A CATALYTIC COMBUSTION SYSTEM FOR THE MIT MICRO GAS TURBINE ENGINE

by

Jhongwoo Peck

Submitted to the Department of Aeronautics and Astronautics
in partial fulfillment of the requirements for the degree of

Master of Science in Aeronautics and Astronautics

ABSTRACT

As part of the MIT micro-gas turbine engine project, the development of a hydrocarbon-fueled catalytic micro-combustion system is presented. A conventionally-machined catalytic flow reactor was built to simulate the micro-combustor and to better understand the catalytic combustion at micro-scale. In the conventionally-machined catalytic flow reactor, catalytic propane/air combustion was achieved over platinum. A 3-D finite element heat transfer model was also developed to assess the heat transfer characteristics of the catalytic micro-combustor. It has been concluded that catalytic combustion in the micro-combustor is limited by diffusion of fuel into the catalyst surface. To address this issue, a catalytic structure with larger surface area was suggested and tested. It was shown that the larger surface area catalyst increased the chemical efficiency. Design guidelines for the next generation catalytic micro-combustor are presented as well.

Thesis Supervisor: Professor Ian A. Waitz

Title: Professor and Deputy Head, Department of Aeronautics and Astronautics

ACKNOWLEDGEMENTS

First of all, I would like to thank Professor Ian Waitz for the best guidance that any graduate student would expect from an advisor. I am also grateful to Professor Alan Epstein for his continuous support and advice. My thanks go to Dr. Stuart Jacobson too for managing such a huge project.

Chris Spadaccini deserves special thanks for being a co-worker, a friend, a writing tutor, and a deputy advisor. I also owe Professor Mark Spearing many thanks for his valuable inputs when designing the catalytic flow reactor. I appreciate Viktor Dubrowski's excellent job in machining the tiny nasty ceramic pieces despite the risk of breaking his machines and getting a lung cancer. The finite element analysis in Chapter 4 would have not been possible without help from Dr. Hyung-Soo Moon. Thank you. Also, I thank Paul Warren for spending tens of hours to install ABAQUS. Jin-wook Lee's generous tips on the micro-combustor are appreciated too. Precious advice from Steve Lukachko has been remarkably helpful throughout the course of the research. Thank you.

Beside the microengine research crew, all the GTL colleagues made the past two years of mine a pleasant time. Thank you guys: Sebastien Aknouche, Keen Ian Chan, Dongwon Choi, Ling Cui, Dr. Dan Kirk, (Big) Joe Lee, Vai Man Lei, Yiben Lin, Jun Luo, David Milanes, Mark Monroe (M²), (Professor) Neil Murray, Deborah Pilczer, Chris Protz (CP), Chiang Juay (CJ) Teo, Yong Wang, and Benny Yam. Since my arrival at MIT, Jihyun has been the closest and dearest companion. Thanks.

I am grateful to all my buddies at the First Korean Church in Cambridge for their prayers and true friendship. I especially thank Colin Joye for proofreading the thesis. I express my sincerest gratitude to Hyejoo for the motivation when writing the thesis.

Mom, Dad, and brother Jongyoon, thank you all for your love, care, encouragement, and sacrifice.

Above all, I thank and praise God for everything He has done, is doing, and will be doing in me and through me.

This work was sponsored by the United States Army Research Office and by DARPA. Their support is gratefully acknowledged.

CONTENTS

1 Introduction	15
1.1 Background	15
1.2 The MIT Microengine	15
1.3 Micro-combustor	16
1.3.1 Requirements and constraints	16
1.4 Previous Research on Micro-combustor	18
1.4.1 Gas-phase micro-combustors: single and dual-zone combustors	18
1.4.2 Catalytic micro-combustors	22
1.5 Motivation for the Present Research	24
1.6 Objectives of the Research	24
1.7 Contributions of the Research	24
1.8 Organization of the Thesis	25
2 Experimental Apparatus Design	27
2.1 Requirements	27
2.2 Apparatus Design	27
2.2.1 Design issues	27
2.2.2 Detailed design	28
2.3 Device Calibration	30
2.3.1 Comparison to baseline six-wafer micro-combustor	30
2.3.2 Gas-phase combustion	31
2.3.3 Thermal resistance analysis	32
2.4 Design Modification	36
2.5 Preparation of Catalytic Insert	38
2.6 Chapter Summary	39
3 Experimental Results	41
3.1 Catalytic Combustion of Hydrocarbon Fuels	41
3.1.1 Catalytic ignition procedure	41
3.1.2 Catalytic combustion of propane over platinum	42
3.2 Catalytic Ignition and Extinction Test Using Hydrogen	44
3.3 Catalytic Combustion over a Denser Catalytic Insert	45
3.3.1 Motivation	45
3.3.2 Procedure	46
3.3.3 Results	46
3.4 Inspection of Used Catalytic Inserts	46
3.5 Chapter Summary	51

4 Numerical Modeling Results	53
4.1 Numerical Tools	53
4.1.1 ABAQUS	53
4.1.2 PATRAN	53
4.2 Calculation Procedure	54
4.2.1 Geometry and grid generation	54
4.2.2 Boundary conditions	54
4.2.3 Calculation procedure	56
4.2.4 Validation of the model	57
4.3 Micro-combustor Results	57
4.3.1 Temperature distribution	57
4.3.2 Efficiency breakdown	58
4.4 Catalytic Flow Reactor Results	59
4.4.1 Temperature distribution	59
4.4.2 Efficiency breakdown	60
4.5 Comparison of Single-density and Double-density Foam	61
4.6 Chapter Summary	61
 5 Conclusions	 63
5.1 Summary of the Experiments and Analyses	63
5.2 Design Suggestions for the Second Generation Catalytic Micro-combustor ...	63
5.3 Continuing Work	64
5.4 Recommendations for Future Work	65
 Appendix A Drawings of Catalytic Flow Reactor	 67
A.1 Top-plate	67
A.2 Middle-plate	68
A.3 Bottom-plate	69

LIST OF FIGURES

Figure 1.1	Cross sectional illustration of microengine showing flow path	16
Figure 1.2	Schematic of baseline six-wafer micro-combustor	19
Figure 1.3	Packaged micro-combustor	19
Figure 1.4	Pre-mixed hydrogen/air combustion results in baseline six-wafer micro-combustor	20
Figure 1.5	Schematic of dual-zone micro-combustor showing flow path	20
Figure 1.6	Fuel injected hydrogen/air combustion results in dual-zone micro-combustor	21
Figure 1.7	Comparison between baseline and dual-zone micro-combustors	21
Figure 1.8	Comparison of results for propane/air combustion and hydrogen/air combustion in gas-phase micro-combustor	22
Figure 1.9	Fabrication, assembly, and bonding process for six-wafer catalytic micro-combustor	23
Figure 1.10	Catalytic pieces being inserted into six-wafer micro-combustor	23
Figure 2.1	Exploded schematics of catalytic flow reactor	29
Figure 2.2	Three dimensional illustration of catalytic flow reactor cross section showing flow path	29
Figure 2.3	Fully assembled catalytic flow reactor	30
Figure 2.4	Complete test facility of catalytic flow reactor	31
Figure 2.5	Calibration of catalytic flow reactor with hydrogen/air combustion.	33
Figure 2.6	Calibration of catalytic flow reactor with ethylene/air combustion ..	33
Figure 2.7	Calibration of catalytic flow reactor with propane/air combustion ..	34
Figure 2.8	Thermal circuit analogies of micro-combustor and catalytic flow reactor	35
Figure 2.9	Modification of fuel/air injector geometry in catalytic flow reactor.	37
Figure 2.10	Modification of thermocouple measurement holes in catalytic flow reactor	37
Figure 2.11	Comparison of modified catalytic flow reactor and baseline gas-phase micro-combustor	38
Figure 2.12	Nickel foam inserts cut into shape of combustion chamber before platinum coating	39
Figure 3.1	Results of catalytic propane/air combustion over platinum insert ...	43
Figure 3.2	Combustor efficiency for catalytic propane/air combustion over platinum insert	43
Figure 3.3	Total pressure loss across combustion chamber for catalytic propane/air combustion with equivalence ratio 0.75	44

Figure 3.4	Catalytic ignition and extinction hysteresis	45
Figure 3.5	Results of catalytic propane/air combustion over double-density platinum insert	47
Figure 3.6	Combustor efficiency for catalytic propane/air combustion over double-density platinum insert	47
Figure 3.7	Comparison of temperature response for single-density and double-density foam experiments	48
Figure 3.8	Comparison of total pressure loss for single-density and double-density foam experiments	48
Figure 3.9	SEM of untreated nickel insert	49
Figure 3.10	SEM's of platinum (coated on nickel) insert before testing	50
Figure 3.11	SEM's of platinum insert after testing	51
Figure 4.1	Replacement of non-axi-symmetric geometry	54
Figure 4.2	Station numbering on micro-combustor geometry showing flow path	56
Figure 4.3	Experimental validation of finite element heat transfer model	58
Figure 4.4	Temperature profile calculated by finite element heat transfer model for micro-combustor geometry	58
Figure 4.5	Efficiency breakdown for micro-combustor	59
Figure 4.6	Temperature profile calculated by finite element heat transfer model for catalytic flow reactor geometry	60
Figure 4.7	Efficiency breakdown for catalytic flow reactor	60
Figure 4.8	Comparison of efficiencies for single-density foam and double-density foam	61
Figure A.1	Mechanical drawing of the top-plate of the catalytic flow reactor ..	67
Figure A.2	Mechanical drawing of the middle-plate of the catalytic flow reactor	68
Figure A.3	Mechanical drawing of the bottom-plate of the catalytic flow reactor	69

LIST OF TABLES

Table 2.1	Comparison of catalytic flow reactor and baseline six-wafer micro-combustor	31
Table 2.2	Thermal resistances in micro-combustor	35
Table 2.3	Thermal resistances in catalytic flow reactor	35
Table 4.1	Overall heat transfer coefficients on each wall of micro-combustor geometry	55

NOMENCLATURE

Roman

D	Characteristic diameter scale (m)
Da	Damköhler number
H	Characteristic height scale (m)
h	Convective heat transfer coefficient (W/m ² K)
k	Thermal conductivity (W/mK)
L	Characteristic length scale (m)
Nu	Nusselt number
P	Pressure (Pa)
Pr	Prandtl number
R	Gas constant (J/kgK), Thermal resistance (K/W)
Re	Reynolds number
r	Characteristic radius scale (m)
T	Temperature (K)
V	Volume (m ³)

Greek

ϕ (or phi)	Equivalence ratio
η	Efficiency

Subscripts

a	Air
f	Fuel

Full quantities

E_a	Activation energy (J/kg)
h_1	Specific enthalpy of inlet gas mixture (J/kg)
h_2	Specific enthalpy of combustion product (J/kg)
h_f	Fuel heating value (J/kg)
\dot{m}	Mass flow rate (g/sec)
\dot{Q}_{loss}	Heat loss (W)
η_{chem}	Chemical efficiency

η_{thermal}	Thermal efficiency
$\eta_{\text{combustor}}$	Overall combustor efficiency
τ_{chem}	Characteristic chemical reaction time (sec)
τ_{res}	Residence time (sec)

Acronyms

MEMS	Micro Electro Mechanical Systems
SEM	Scanning Electron Microscope

CHAPTER 1

INTRODUCTION

1.1 BACKGROUND

MIT initiated a research program seven years ago to develop the technology for micro gas turbine generators that can ultimately produce 10-100 watts of electrical power within a package less than one cubic centimeter in volume [2]. The resulting power density would be in excess of $2,300\text{MW/m}^3$, which is at least an order of magnitude higher than that of other existing power MEMS devices, and over ten times the power density of the best batteries available to date. Based on a gas turbine Brayton cycle, the MIT microengine contains all the functional components of a conventional gas turbine engine. However, its small scale imposes new challenges which include the development of low Reynolds number turbomachinery, high-efficiency micro-combustors, high-load air bearings, high power microelectronic generators, and silicon and silicon carbide micro-fabrication techniques. Thus, the work is divided into eight principal areas: (1) engine systems design, (2) turbomachinery fluid dynamics, (3) combustion, (4) structures, (5) bearings, (6) electrical machinery, (7) silicon fabrication technology, and (8) microfabrication of high temperature materials and structures. The thesis focuses on the development of a catalytic combustion system for the MIT microengine.

1.2 THE MIT MICROENGINE

Although the only imposed requirement is that the microengine outperforms other existing compact power sources such as batteries, Epstein et al. have defined the general goals of the engine design [2]:

- Thrust consistent with a power output of several watts or more
- Engine life of tens of minutes or more
- A design with a minimum number of stacked wafers
- A design with growth potential

With these requirements in mind, detailed functional specifications were set, and a layout was suggested. Figure 1.1 shows the cross section of the microengine. Air comes in through the inlet and makes a right angle turn into a compressor, where it is compressed up to 2-3 atm. Fuel is then injected, and the fuel and air mixture passes through a recirculation jacket. The fuel and air mixture enters the combustor from the bottom, and chemical reactions occur in the combustor. As a result, the gas temperature is raised to approximately 1600K. Finally, the combustion products pass through a turbine before leaving the engine. The power extracted from the turbine drives the compressor.

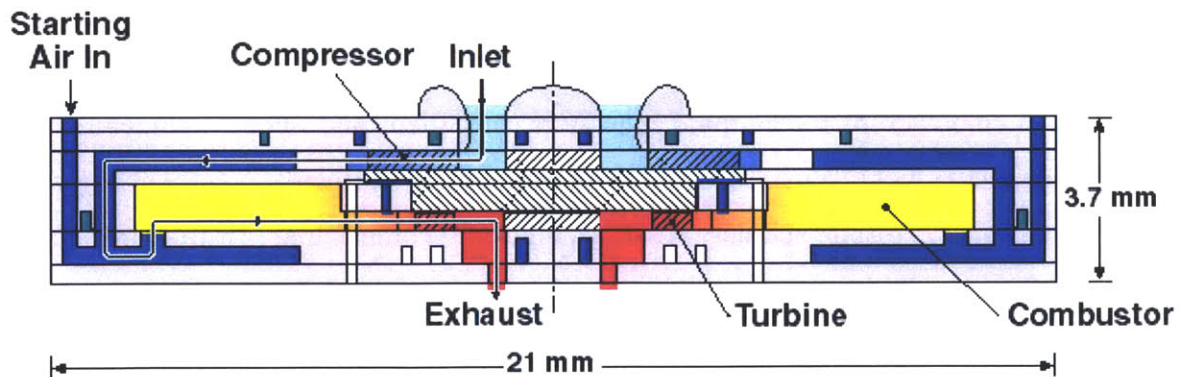


Figure 1.1: Cross sectional illustration of microengine showing flow path

1.3 MICRO-COMBUSTOR

1.3.1 Requirements and Constraints

In order for the micro-combustor to be operable in the MIT micro gas turbine engine, there exist several functional requirements [10]. Chemical energy should be converted

into thermal and kinetic energy with high efficiency, desirably higher than 90%. To close the microengine thermodynamic cycle, the total pressure drop across the combustor must be less than 5%, and the temperature of the combustor exhaust should be higher than 1600K. It should be easily ignitable and stable.

Meeting these requirements is not trivial because of constraints including chemical kinetics, thermal performance of materials, and micro-fabrication issues [10]. Since high power density is desired, which is proportional to the mass flow rate through a given combustor volume, the residence time of the gas mixture in the combustor becomes inevitably short. Eq. 1.1 explains this trend.

$$\tau_{res} \approx \frac{\text{volume}}{\text{volume flow rate}} = \frac{VP}{\dot{m}RT} \propto \frac{1}{\text{power density}} \quad \text{<Eq. 1.1>}$$

Whereas the residence time in conventional combustors is typically an orders of magnitude longer than the chemical reaction time. This is not the case in a micro-system. Eq. 1.2 indicates that the kinetic rates are not a function of size.

$$\tau_{chem} \approx \frac{[fuel]}{A[fuel]^a[O_2]^b e^{-E_a/RT}} \quad \text{<Eq. 1.2>}$$

The chemical/residence time constraints are often quantified by the Damköhler number, which is the ratio of residence time to the chemical reaction time.

$$Da = \frac{\tau_{res}}{\tau_{chem}} \quad \text{<Eq. 1.3>}$$

There are heat transfer challenges as well. The micro-combustor loses much heat through the surface due to its large surface area-to-volume ratio at micro-scale. Whereas conventional combustors have 3 to 5 m⁻¹ surface area-to-volume ratio, the micro-combustor has approximately 500 m⁻¹. The large surface area-to-volume ratio compromises the combustor efficiency. It may lead to quenching of reactions at walls, and thus increase the chemical reaction time. In addition, due to the presence of short

heat conduction paths, heat transfer is controlled by convection. Therefore, the structure is nearly isothermal. This has advantages by reducing thermal stresses in parts of the structure, but lowers the compressor efficiency by adding irreversibility to the cycle. In summary, coupling between fluid dynamics, heat transfer, and chemical kinetics is more significant for micro-combustion systems.

1.4 PREVIOUS RESEARCH ON MICRO-COMBUSTOR

1.4.1 Gas-phase Micro-combustors: Single and Dual-zone Combustors

With all the requirements and constraints in mind, a baseline six-wafer micro-combustor shown in Figures 1.2 and 1.3 was designed, fabricated, and tested. The baseline six-wafer micro-combustor has all the engine components except the rotating spool at the center. Hydrogen and such hydrocarbons as ethylene and propane were tested in this device. Shown in Figure 1.4 is a result from the baseline six-wafer micro-combustor. More detailed description and analysis may be obtained from the Mehra [10]. The baseline six-wafer micro-combustor satisfies the exhaust gas temperature requirement of 1600K, but fails to operate at the design mass flow rate of 0.2g/sec for 225 μ m blade heights.

In an effort to improve performance, a dual-zone micro-combustor was developed by Spadaccini [12]. The design was modified so that a series of holes allowed a portion of inlet air to flow directly into the combustion chamber without passing through the recirculation jacket. This dilution air is mixed with the hot combustion products after the primary zone, where the chemical reactions occur in a richer fuel/air mixture and at higher temperatures. This results in increased kinetic rates and thus higher local Damköhler numbers. The cross sectional view of the dual-zone micro-combustor and the results from the device are shown in Figures 1.5 and 1.6 respectively.

The dual-zone micro-combustor almost doubled the mass flow rate capability as shown in Figure 1.7, so the required flow rate and exhaust gas temperature are both met when using hydrogen. However, tests with hydrocarbon fuels show that the dual-zone micro-combustor will not be able to burn hydrocarbons at the design mass flow rate. Shown in Figure 1.8 is the comparison of the best propane result and the hydrogen result. It can be seen that there is almost a 5-fold difference between the two fuels. This is due to their kinetic rates.

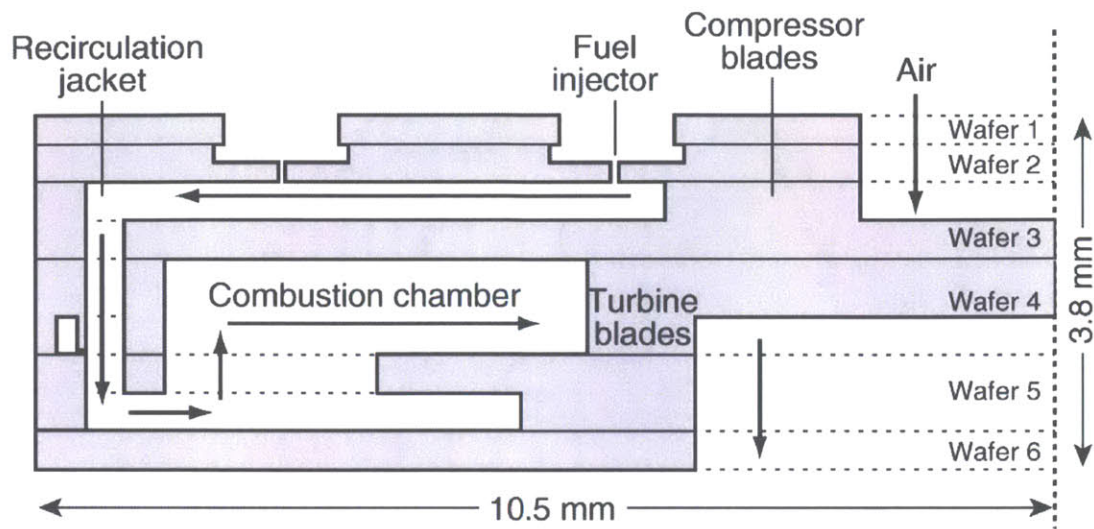


Figure 1.2: Schematic of baseline six-wafer micro-combustor (Mehra [10])

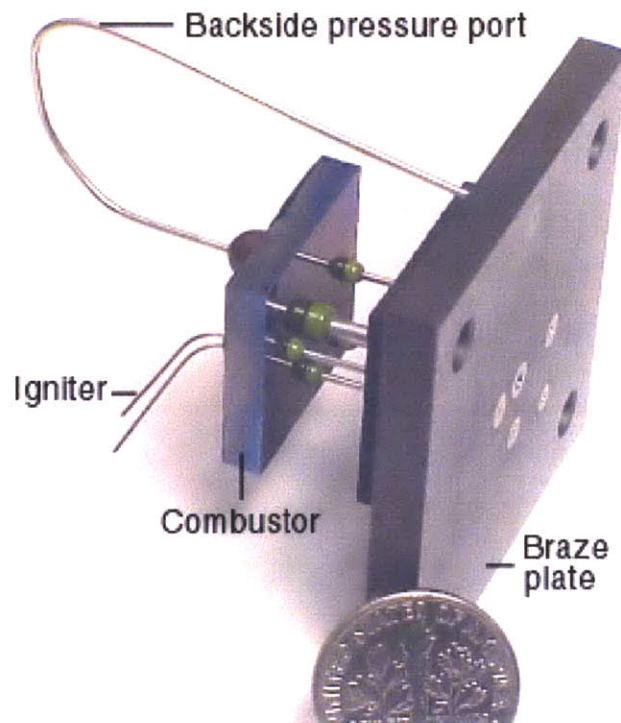


Figure 1.3: Packaged micro-combustor (Mehra [10])

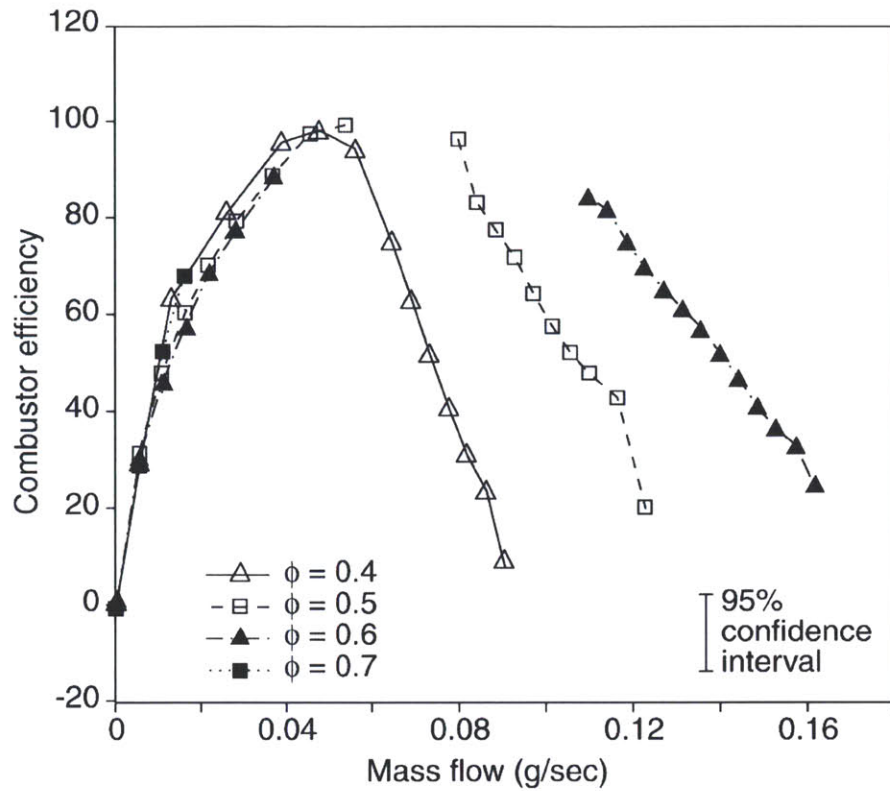


Figure 1.4: Pre-mixed hydrogen/air combustion results in baseline six-wafer micro-combustor (Mehra [10])

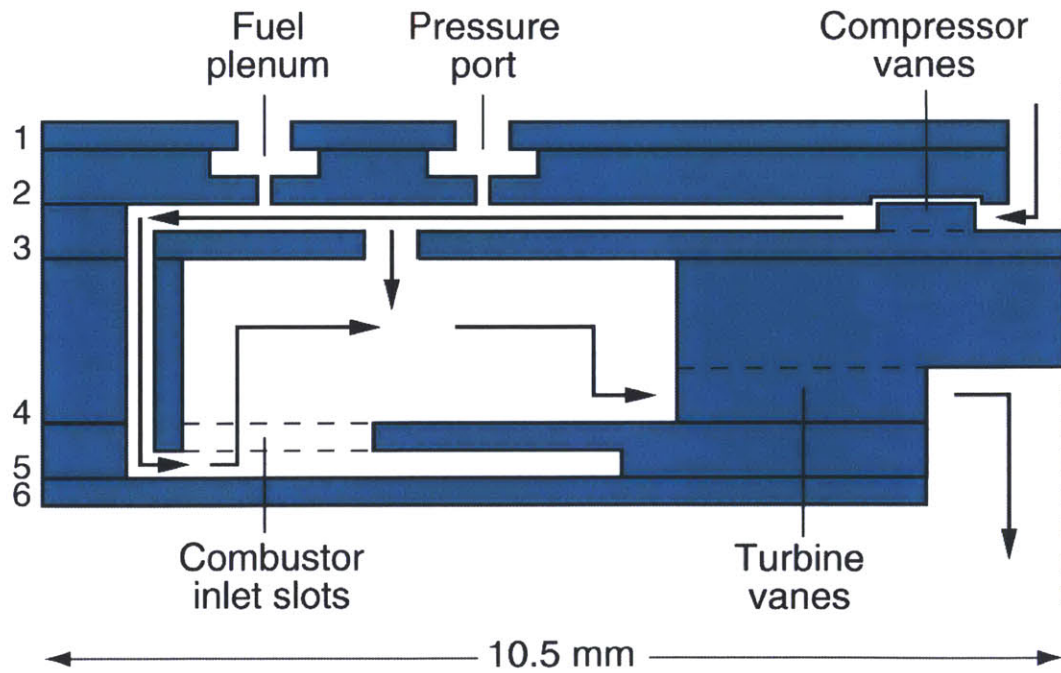


Figure 1.5: Schematic of dual-zone micro-combustor showing flow path (Spadaccini [12])

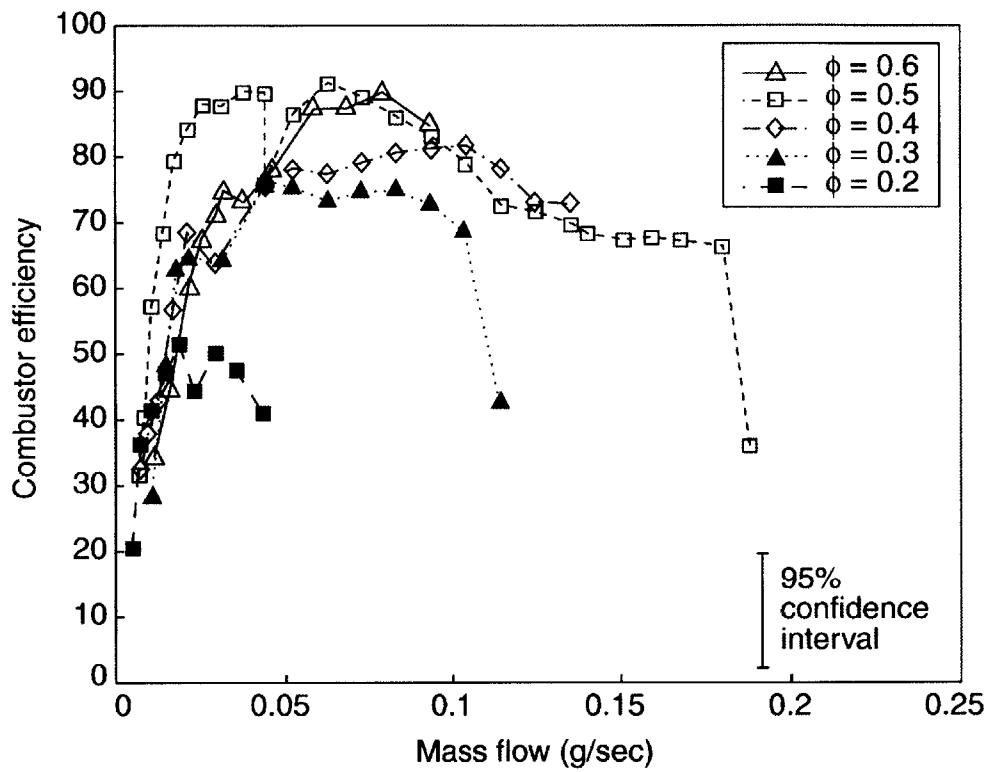


Figure 1.6: Fuel injected hydrogen/air combustion results in dual-zone micro-combustor (Spadaccini [12])

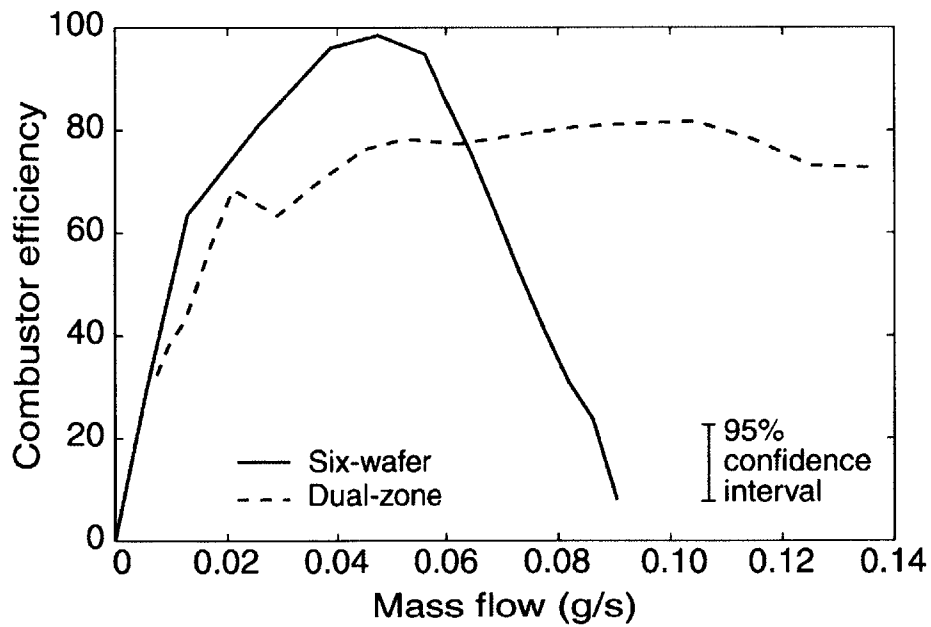


Figure 1.7: Comparison between baseline and dual-zone micro-combustors. (Hydrogen, $\phi=0.4$, Spadaccini [12])

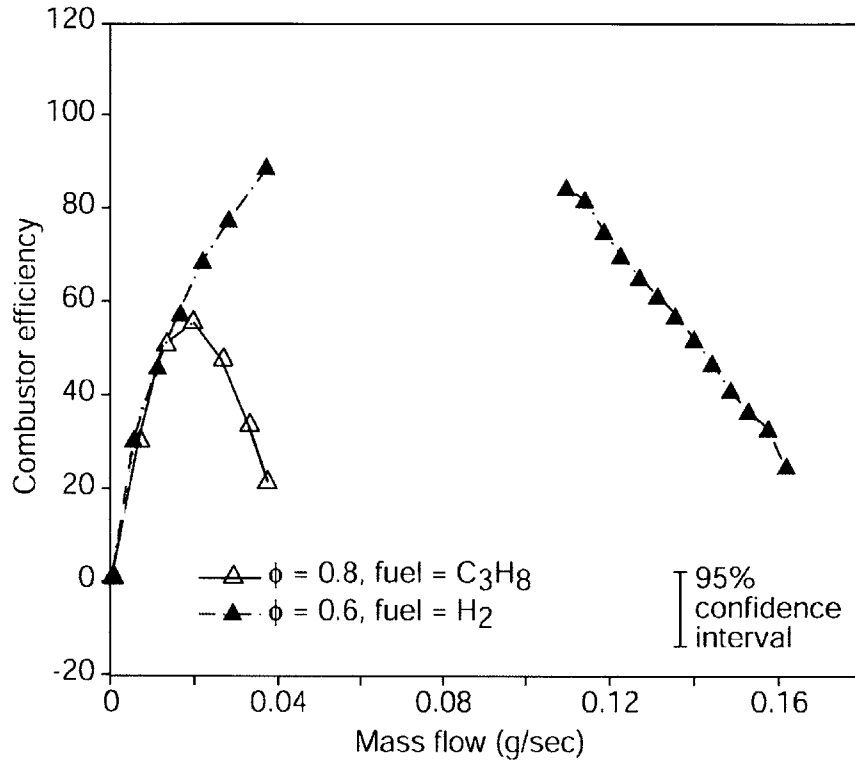


Figure 1.8: Comparison of results for propane/air combustion and hydrogen/air combustion in gas-phase micro-combustor (Spadaccini [14])

1.4.2 Catalytic Micro-combustors

Analyses and experiments to date suggest that homogenous gas-phase hydrocarbon/air combustion will not be possible at the desired design flow rate and combustor volume. Therefore, surface catalysis was suggested as a possible improvement because it may improve stability, ignition characteristics, and reaction rates. However, there also exist several issues associated with catalytic combustion. First, durability of catalysts at such high temperatures is questionable. The structural temperatures are expected to be higher. In addition, complicated flow paths due to the existence of a foreign structure in the combustion chamber will increase the pressure loss across the combustor. Whether the pressure loss will remain within the requirement is in question. There are fabrication issues as well. Incorporating the catalyst into the micro-fabrication process poses several challenges to bonding, including surface contamination, surface damage, and wafer bow. A detailed explanation of the micro-fabrication process can be found in the Spadaccini et al. [13].

Despite these challenges, the six-wafer catalytic micro-combustor was successfully fabricated. As shown in Figure 1.9, it looks identical to the baseline six-wafer micro-combustor except that it has catalytic foam occupying the combustion chamber (See Figure 1.10). Platinum plated nickel foam was used since platinum is known to be a good catalyst for hydrocarbon combustion. A more detailed description about preparing the catalytic substrate will be presented in Chapter 2.

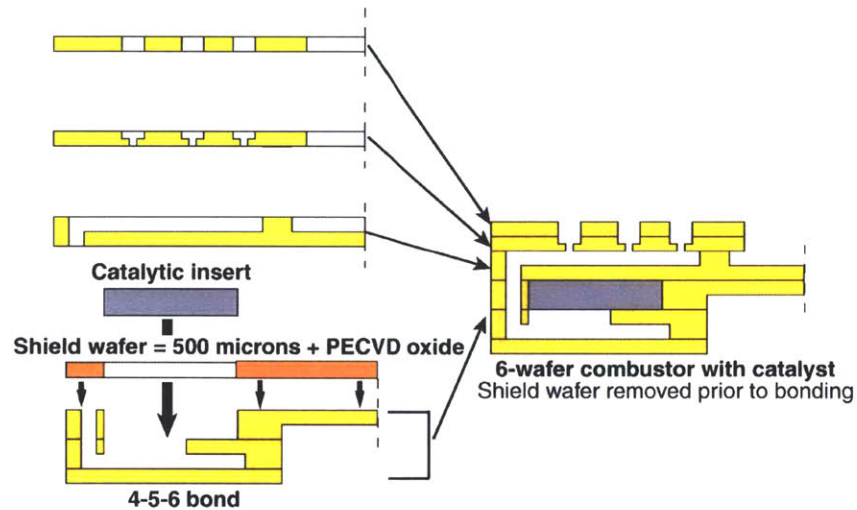


Figure 1.9: Fabrication, assembly, and bonding process for six-wafer catalytic micro-combustor (Spadaccini [13])

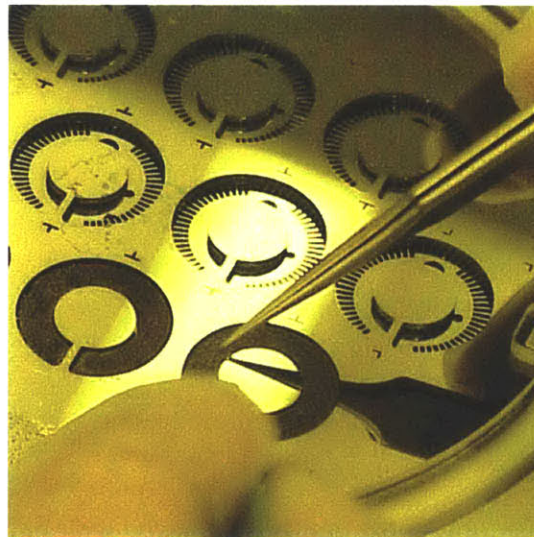


Figure 1.10: Catalytic pieces being inserted into six-wafer micro-combustor (Spadaccini [13])

1.5 MOTIVATION FOR THE PRESENT RESEARCH

Previous research identified a need for the use of surface catalysis in order for micro-combustors to meet the design requirements of the MIT microengine. Accordingly, six-wafer catalytic micro-combustors have been successfully fabricated and packaged despite several issues mostly associated with the micro-fabrication processes. Since the catalytic micro-combustor is the first of its kind, its performance over a range of conditions is unknown. Before testing the valuable six-wafer catalytic micro-combustors, it would be instructive to evaluate catalyst operability and durability in a similar environment. A decision was made to build a conventionally-machined flow reactor that can simulate the environment within the micro-combustors.

1.6 OBJECTIVES OF THE RESEARCH

The objective of the present research is to develop reliable design tools for the catalytic micro-combustor by utilizing both experimental and numerical methods. Catalyst operating space and failure modes were assessed in the catalytic flow reactor to provide guidelines for the micro-combustor without damaging the valuable devices. Then a numerical heat transfer model was used to explore the heat transfer characteristics of the catalytic micro-combustor. These results, along with the experimental data obtained in the catalytic micro-combustors, were used to define the problems and shortcomings of the current design. Finally, design suggestions for the second generation catalytic micro-combustor were presented.

1.7 CONTRIBUTIONS OF THE RESEARCH

The key contributions of the research are:

- (1) A conventionally-machined catalytic flow reactor was built.
- (2) Catalytic propane/air combustion was achieved over platinum in the micro-combustor geometry.

- (3) A 3-D finite element heat transfer model was developed to characterize the heat transfer property of the catalytic micro-combustor.
- (4) A conclusion that the combustion process in the catalytic micro-combustor is limited by the diffusion of the fuel was drawn assisted by the results from the research.
- (5) A new design concept of using denser foam was suggested and tested.
- (6) Guidelines for the next generation catalytic micro-combustor were presented.

1.8 ORGANIZATION OF THE THESIS

This chapter introduces the concept of the MIT micro gas turbine engine and the micro-combustor including the gas-phase and the catalytic micro-combustors. Key objectives and contributions were also stated.

Chapter two describes the effort to build a conventionally-machined catalytic flow reactor that can be used to simulate the catalytic micro-combustor.

Chapter three summarizes the results from the catalytic flow reactor. It presents the results of catalytic propane/air combustion over platinum inserts, catalytic ignition/extinction hysteresis, and some preliminary results with a denser substrate. It presents SEM images of inserts as well.

Chapter four summarizes a modeling effort. A 3-D finite element heat transfer analysis is conducted to better understand the heat transfer characteristics of the micro-combustor, and the results are presented in this chapter.

Chapter five presents the conclusion of this thesis along with on-going work and recommendations for future work.

CHAPTER 2

EXPERIMENTAL APPARATUS DESIGN

2.1 REQUIREMENTS

The primary objectives of building the catalytic flow reactor are to provide a preliminary evaluation of the catalyst operating space and to investigate the failure modes. In addition to this, information regarding long-term durability will be obtained. Long-term objectives include evaluating other catalysts and catalyst support materials. Once design suggestions for the next generation catalytic micro-combustor are made, the flow reactor will also be used to verify the concepts. It will be used to validate the 3-D finite element heat transfer model as well.

To accomplish these objectives, it is desirable for the reactor to have similar boundary conditions as the catalytic micro-combustors. It should have approximately the same volume, flow-path, and chamber pressures as the micro-fabricated device. Moreover, the reactor should utilize the existing facilities such as the fuel/air supply system, instrumentation, and the data acquisition system. Since several different catalytic materials will be tested in the reactor, its parts should be easily disassembled for replacement of the catalytic inserts.

2.2 APPARATUS DESIGN

2.2.1 Design Issues

As stated in the requirements, the wall temperature of the micro-combustor can exceed 800K. The reactor should have the ability to function at this high temperature while still

being fabricated conventionally. Machineable glass ceramic, or MACOR®, was selected for the body material [15]. MACOR® is a white ceramic which can be machined with ordinary steel or carbide tools and can be used at temperatures up to 1000K [4]. Since the reactor must consist of several components that can be disassembled easily, sealing can be an issue. Flexible graphite, or Grafoil®, was utilized as a gasket material due to its high temperature durability of 3000°C [5] and resilient nature [15].

2.2.2 Detailed Design

Figure 2.1 shows exploded views of the flow reactor. Figures 2.2 and 2.3 show the cross section of the flow reactor and the assembled rig respectively. The mechanical drawings of each part are included in Appendix A. The dimensions of the flow reactor's combustion chamber were determined based on those of the micro-combustor. The combustion chamber is 1mm in height, 18.4mm in outer diameter, and 9.6mm in inner diameter. There is a top-plate, which has a fuel/air inlet and a fuel plenum. A middle-plate separates the fuel plenum and the combustion chamber. Twenty-four fuel/air injection holes, each of which is 0.014in across, are located on the middle-plate. A bottom-plate forms the combustion chamber where the catalytic insert is placed. The device is designed only for premixed combustion. Premixed fuel/air enters the plenum through the inlet. Then, a fuel/air mixture is injected into the combustion chamber through the twenty-four fuel/air injection holes. The combustion process occurs as the mixture goes radially inward from the injectors to an exhaust channel. The exhaust channel has an area similar to that of the micro-combustor, and is supposed to choke the flow at the design mass flow rate. Comparing the flow path with that of the micro-combustor, it is quite similar in that the flow path is radially inward. The major discrepancy is that the flow reactor does not have a recirculation jacket. It is due to the limitation of conventional machining at such a small scale. The lack of the recirculation jacket can make a difference in the boundary conditions or the condition of the fuel/air mixture at the combustion chamber inlet. To minimize the effects of these differences, an external radiative heater was used to control the wall temperature independently. A heated inlet tube, which is a serpentine metal tube electrically heated as shown in Figure

2.4, was also used at the fuel/air inlet to control the temperature of the entering fuel/air mixture [9].

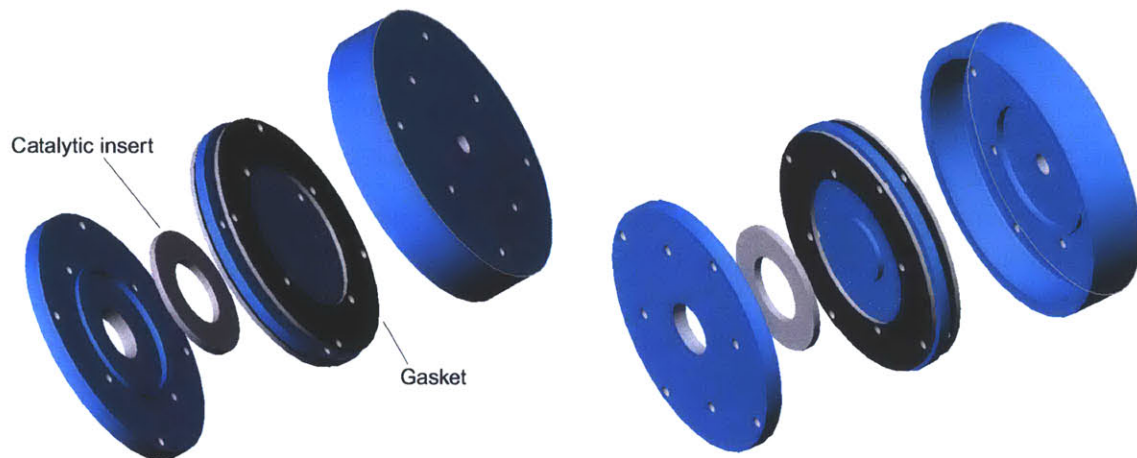


Figure 2.1: Exploded schematics of catalytic flow reactor

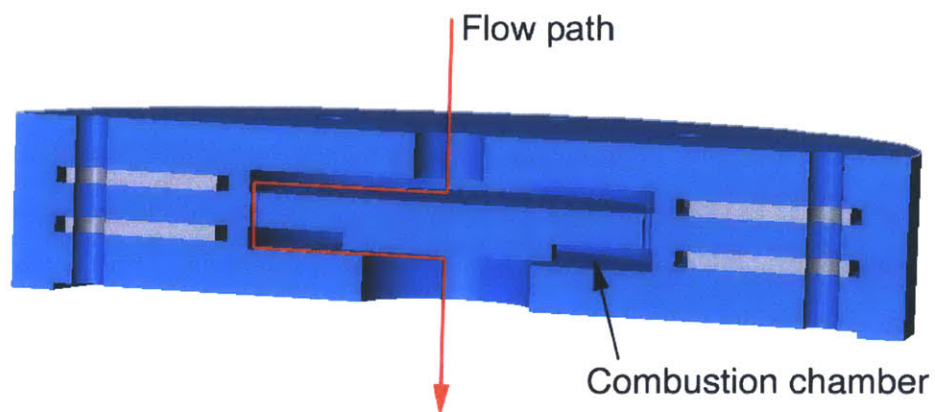


Figure 2.2: Three dimensional illustration of catalytic flow reactor cross section showing flow path

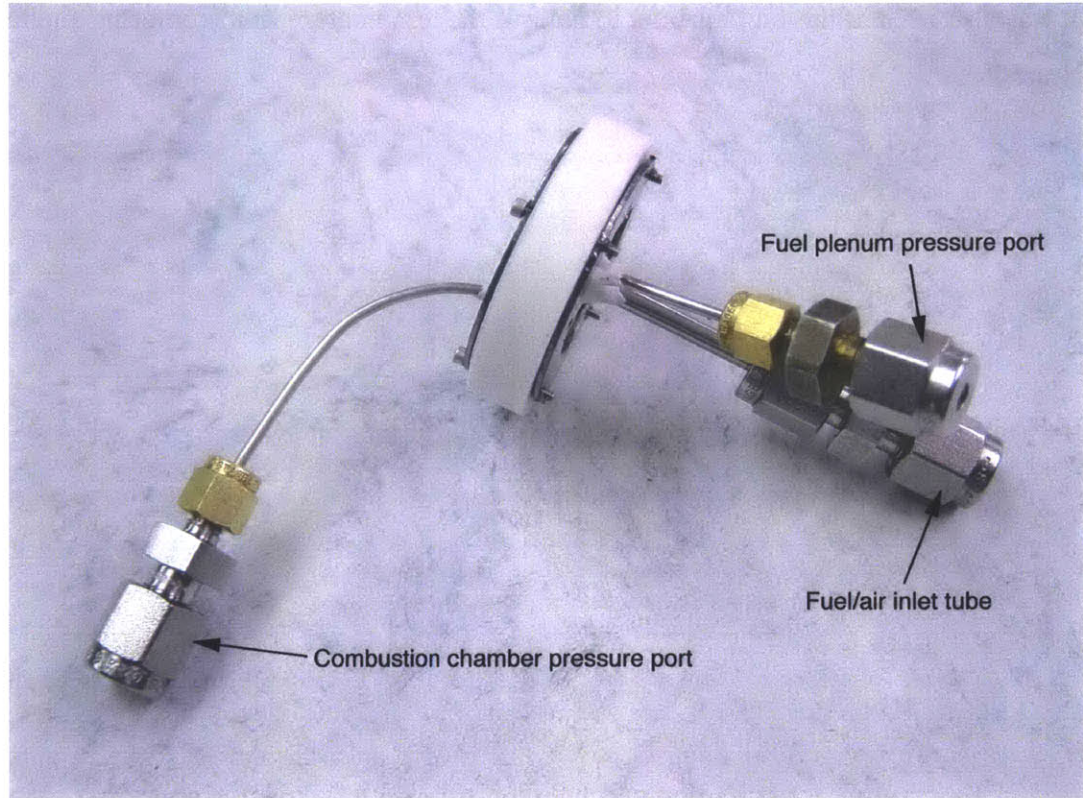


Figure 2.3: Fully assembled catalytic flow reactor

2.3 DEVICE CALIBRATION

2.3.1 Comparison to Baseline Six-wafer micro-combustor

Shown in Table 2.1 are the geometric differences between the catalytic flow reactor and the baseline six-wafer micro-combustor. The volume of the combustion chamber and exit area are almost the same. On the other hand, there exists a slight discrepancy in inlet and exit geometry due to the limitation of conventional machining. Further, overall device size, exterior area, the thermal conductivity of materials, and the presence of a recirculation jacket are different. As discussed in 2.2.2, an external heater and a heated inlet tube were utilized to minimize the effect. The external heater can heat the device to 300°C, and the heated inlet tube can raise the temperature of the gas mixture up to 150°C. Figure 2.4 shows the complete test facility with the external heater and the heated inlet tube.

Table 2.1: Comparison of catalytic flow reactor and baseline six-wafer micro-combustor

	Baseline micro-combustor	Catalytic flow reactor
Combustor volume	190mm ³	194mm ³
Inlet geometry	Slots	Holes
Exit geometry	Nozzle guide vanes	Channel
Exit area	12mm ²	15mm ²
Overall device size	21×21×3.8(mm)	φ40.3×7(mm)
Exterior area	1200mm ²	3450mm ²
Thermal conductivity	125W/mK	1.5W/mK
Recirculation jacket	Yes	No

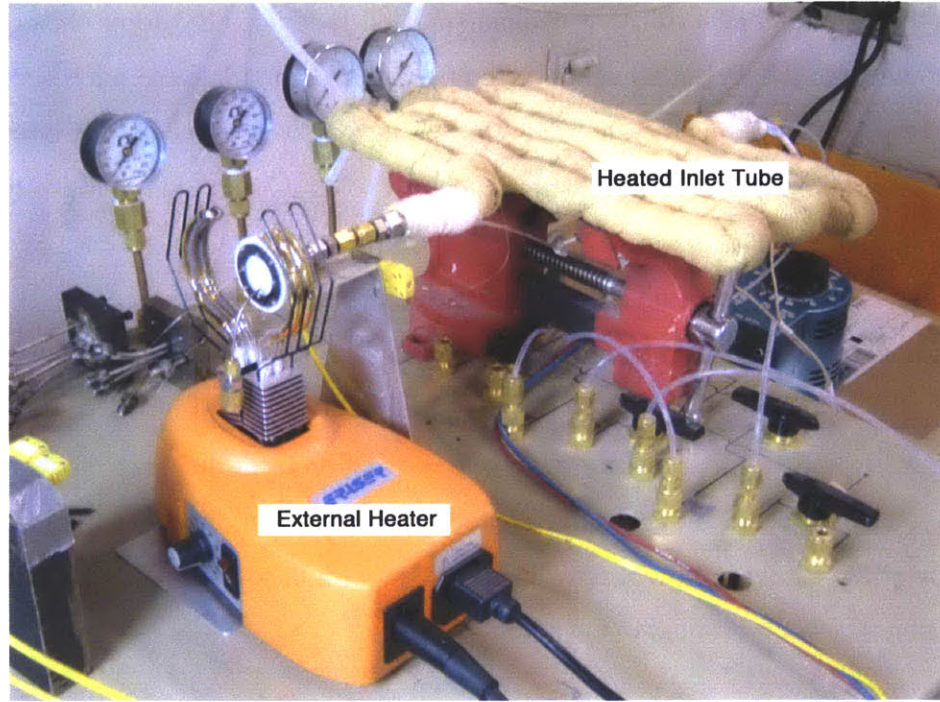


Figure 2.4: Complete test facility of catalytic flow reactor

2.3.2 Gas-phase Combustion

To assess whether the flow reactor simulates the micro-combustor, homogenous gas-phase combustion without any insert in the combustion chamber was tested. The results were compared with the gas-phase combustion results in the baseline six-wafer micro-combustor. Figures 2.5, 2.6, and 2.7 are the comparison between the flow reactor and the six-wafer micro-combustor. All the uncertainty bars represent the 95%-confidence

uncertainty. In general, the catalytic flow reactor had lower exit gas temperature. This is due to the larger heat loss in the catalytic flow reactor. Although the curves for the flow reactor and the micro-combustor are not identical, they match fairly well and the results obtained in the flow reactor may be arguably applicable to the micro-combustor. However, the performance was improved upon following design modifications discussed in Section 2.4.

2.3.3 Thermal Resistance Analysis

In order to understand the heat transfer in the catalytic flow reactor and in the micro-combustor, an electric circuit analogy was utilized [6]. The objective was to evaluate which is the dominant heat transfer mechanism in each device. By doing this, one can manage heat flows better, and thus make the flow reactor simulate the micro-combustor more closely. Figure 2.8 is the diagram representing the analogous electric circuits of the flow reactor and the micro-combustor. Listed in Tables 2.2 and 2.3 are the values of the thermal resistances. The thermal resistances in both circuits are for the case of hydrogen/air combustion at the mass flow rate 0.05g/sec and the equivalence ratio 0.5. By looking at the fraction of each thermal resistance, conduction across the structure has the highest resistance in the catalytic flow reactor, making it the limiting heat transfer mechanism. Relatively low resistance for the convection from the gas to the wall (R_1) in the catalytic flow reactor indicates that more heat is being lost; the lower thermal efficiency of the catalytic flow reactor is consistent with this. More intensive discussion of the efficiencies is presented in Chapter 4.

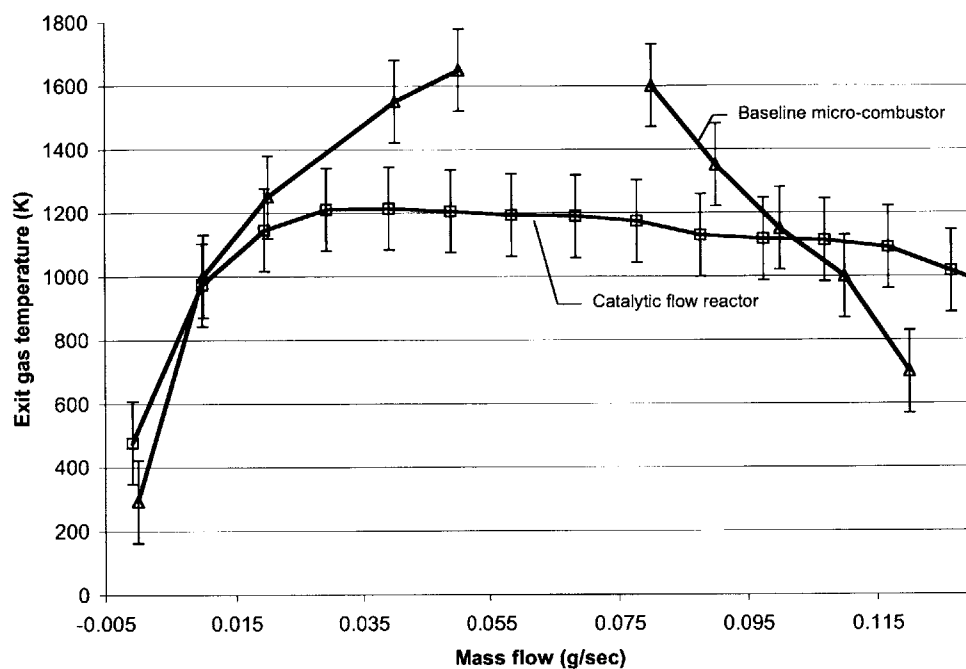


Figure 2.5: Calibration of catalytic flow reactor with hydrogen/air combustion, $\phi=0.5$

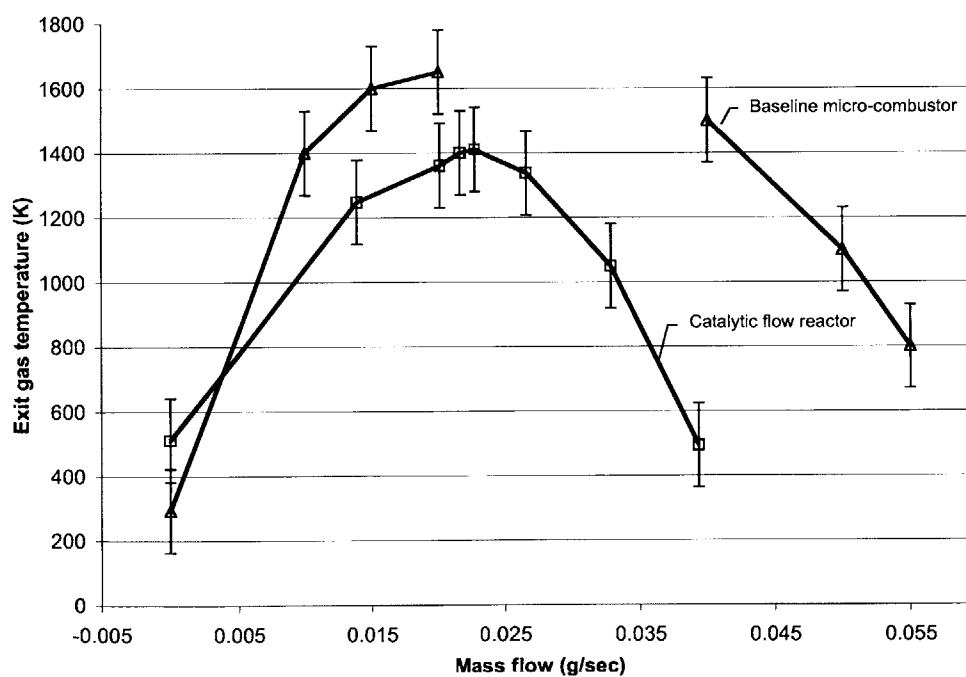


Figure 2.6: Calibration of catalytic flow reactor with ethylene/air combustion, $\phi=0.7$

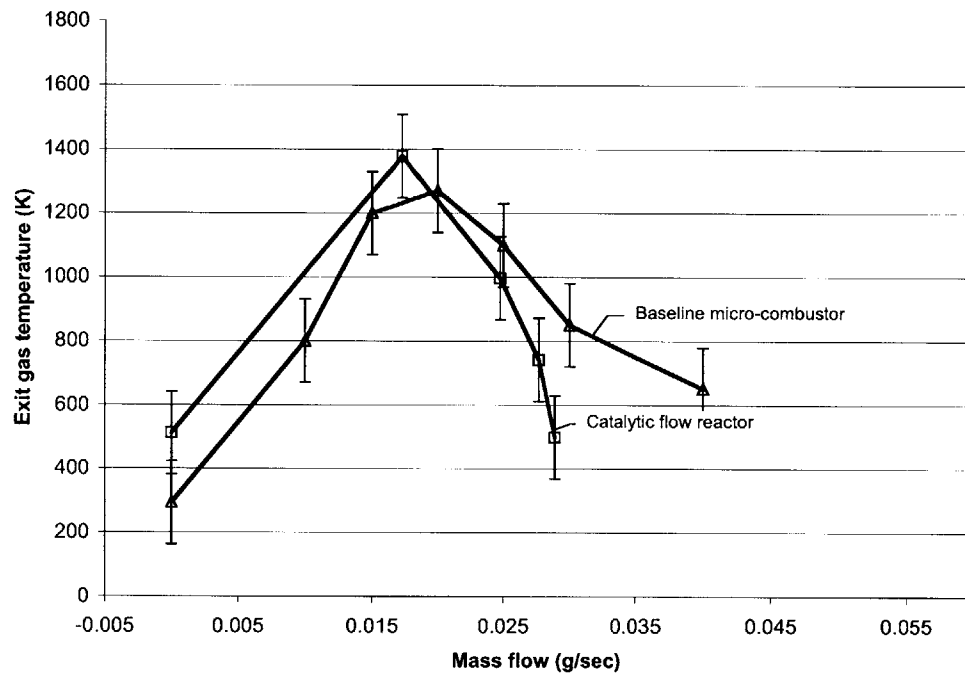
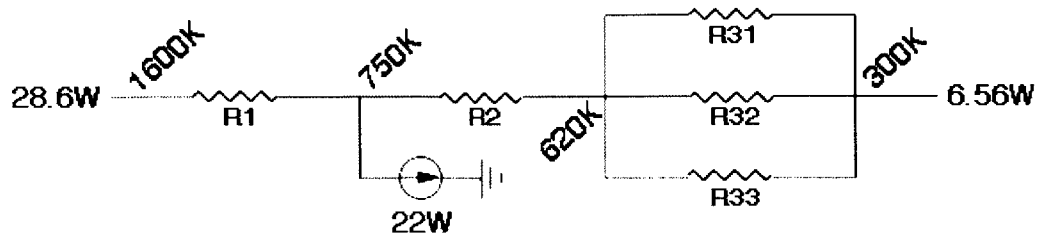
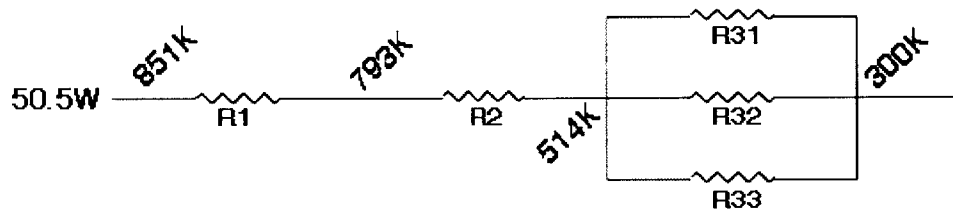


Figure 2.7: Calibration of catalytic flow reactor with propane/air combustion, $\phi=0.8$



<Micro-combustor>



<Catalytic flow reactor>

Figure 2.8: Thermal circuit analogies of micro-combustor and catalytic flow reactor

Table 2.2: Thermal resistances in micro-combustor

R_1	Convection from gas to wall	29.7 K/W	30.2%
R_2	Heat from inner wall to outer wall	19.8 K/W	20.2%
R_{31}	Conductive heat loss	∞	$(R_3 = 48.7)$ 49.6%
R_{32}	Convective heat loss	71.7 K/W	
R_{33}	Radiative heat loss	152 K/W	

Table 2.3: Thermal resistances in catalytic flow reactor

R_1	Convection from gas to wall	1.15 K/W	10.5%
R_2	Conduction across wall	5.52 K/W	50.6%
R_{31}	Conductive heat loss	42.8 K/W	$(R_3 = 4.24)$ 38.9%
R_{32}	Convective heat loss	14.4 K/W	
R_{33}	Radiative heat loss	6.99 K/W	

2.4 DESIGN MODIFICATION

After a series of preliminary experiments in the catalytic flow reactor, several issues were discovered.

- (1) The fuel/air injectors were too small so that the flow appeared to be twenty-four independent jets rather than a body of gas flowing smoothly [8].
- (2) Temperature measurement accessibility was limited.

The injector holes were initially small due to machining limitation. However, with the help of carbide drill bits [3], the injector holes could be enlarged to better simulate the micro-combustor geometry. The modification is shown in Figure 2.9.

Temperature measurements had been planned at similar locations as in the micro-combustor. Considering that the flow reactor has more flexibility in drilling the thermocouple measurement holes, a design modification was made in such a way that one can measure the exhaust gas temperature at four different circumferential locations and the structural temperature at six circumferentially/radially different locations. The enhanced ability to measure temperature distribution across the device enables one to use it to validate the 3-D finite element heat transfer model that will be discussed in Chapter 4. Shown in Figure 2.10 are the new thermocouple measurement locations. Blue marks represent the exhaust gas temperature measurement holes, and red marks correspond the structural temperature measurement holes.

All the results presented henceforth are from the modified device. Compared to Figure 2.5, Figure 2.11 indicates that the modified design better matches the micro-combustor.

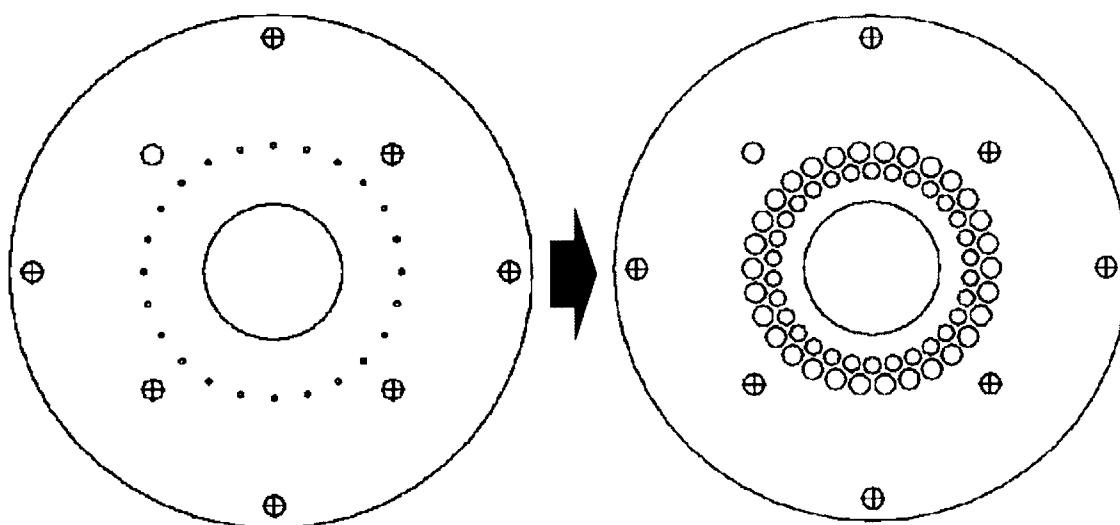


Figure 2.9: Modification of fuel/air injector geometry in catalytic flow reactor

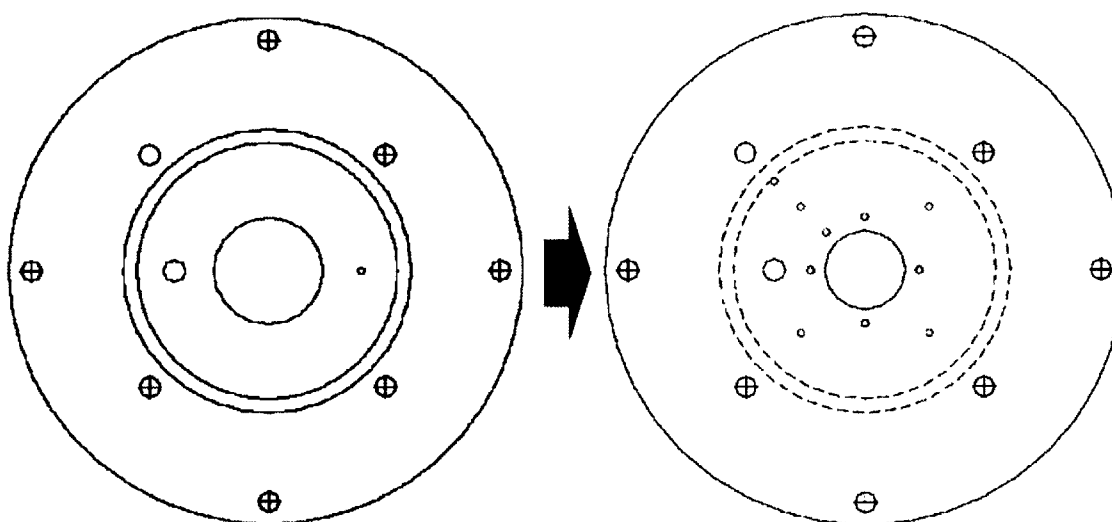


Figure 2.10: Modification of thermocouple measurement holes in catalytic flow reactor

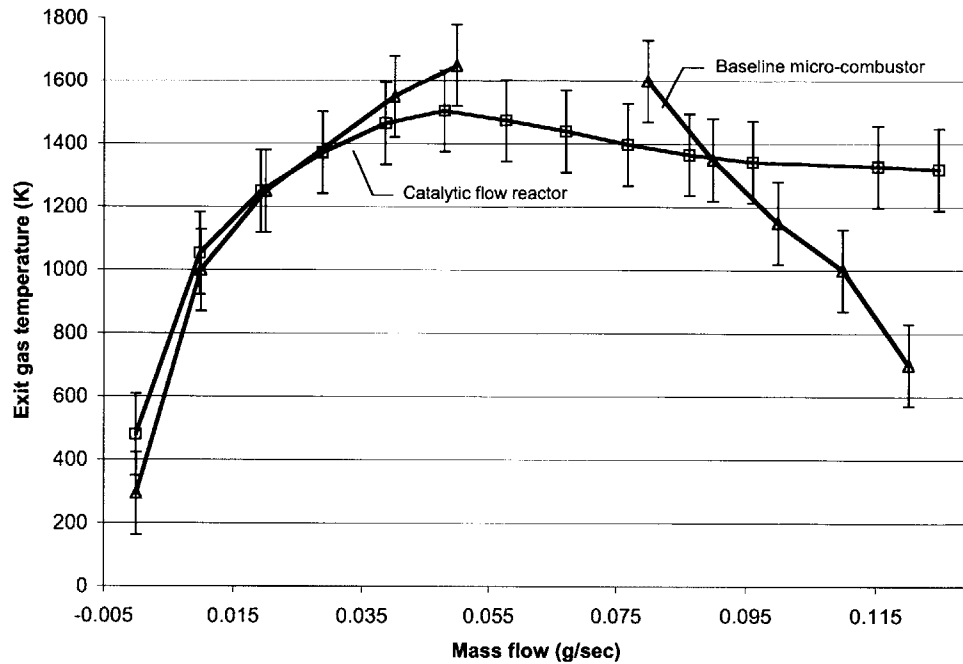


Figure 2.11: Comparison of modified catalytic flow reactor and baseline gas-phase micro-combustor (hydrogen, $\phi=0.5$)

2.5 PREPARATION OF CATALYTIC INSERT

The inserts were prepared by coating platinum on nickel foam cut out of a bulk sheet into the shape of the combustion chamber. The bulk foam sheet was 94% porous by volume according to the vendor. A typical coating process was

- (1) Clean the nickel substrate ultrasonically.
- (2) Dissolve 2.5g of dihydrogen hexachloroplatinate(IV) salt($\text{H}_2\text{PtCl}_6 \cdot 6\text{H}_2\text{O}$) into 20mL of de-ionized water. This makes 12.5% platinum solution.
- (3) Soak the nickel substrate in the solution for about 10 minutes.
- (4) Dry the substrates in a reducing furnace.
 - Run N_2 at 100°C for 2 hours to remove H_2O .
 - Run H_2 at 300°C for 2 hours to remove Cl.

The inserts were weighed before and after the coating procedure, so that the amount of platinum coated could be tracked. Generally, the weight increased by about 10% after coating. Figure 2.12 gives an idea how the inserts look.

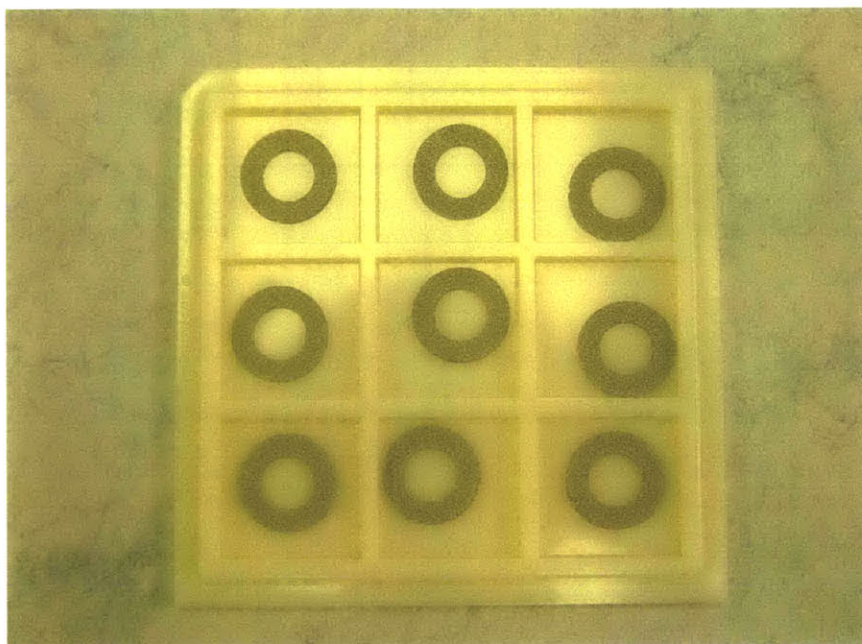


Figure 2.12: Nickel foam inserts cut into shape of combustion chamber before platinum coating.

2.6 CHAPTER SUMMARY

A catalytic flow reactor was built by conventional machining to understand catalyst operability and durability. Eventually, the catalytic flow reactor will be utilized as a design tool for the second generation catalytic micro-combustor along with a 3-D finite element heat transfer model. The flow reactor was calibrated with the baseline six-wafer gas-phase micro-combustor giving fairly good results, which supports using it as a test-bed to predict the performance of the micro-combustor, and to provide guidelines when testing the micro-combustor.

CHAPTER 3

EXPERIMENTAL RESULTS

3.1 CATALYTIC COMBUSTION OF HYDROCARBON FUELS

3.1.1 Catalytic Ignition Procedure

To initiate the catalytic reaction, the catalyst surface temperature must be raised above a certain limit [17]. Catalytic hydrogen/air combustion was first stabilized in the combustion chamber, and then the fuel was slowly converted to propane. The detailed procedure follows:

- (1) Heat the catalytic flow reactor to 200°C using the external heater.
- (2) Flow hydrogen/air mixture, observe ignition, and allow the combustor to stabilize.
(Typically, the equivalence ratio is set at 0.4, and the mass flow rate at 0.02g/sec)
- (3) Turn off the heater. (The catalytic hydrogen combustion brings the temperature of the device up to approximately 410°C.)
- (4) Introduce propane at the equivalence ratio of 0.5. Addition of propane gives an extra temperature rise by about 150°C.
- (5) Slowly reduce hydrogen and increase propane flow rates

- (6) Eventually shut down hydrogen. The auto-thermal propane/air combustion is stabilized.

3.1.2 Catalytic Combustion of Propane over Platinum

Following the above-mentioned procedure, auto-thermal propane/air catalytic combustion could be stabilized in the catalytic flow reactor. The results are shown in Figures 3.1 and 3.2. In Figure 3.1, the horizontal axis represents the mass flow rate in g/sec, and the vertical axis is the temperature measured in Kelvin. The 95%-confidence uncertainty is $\pm 130\text{K}$ for the gas temperatures and $\pm 12\text{K}$ for the structural temperatures. These uncertainties are applied to all the temperature plots presented in Chapter 3. A detailed description of uncertainty analysis can be found in the Mehra [10]. In Figure 3.2, the vertical axis represents the overall combustor efficiency.

The mass flow rate capability was enhanced almost by 10-fold relative to the gas-phase combustion results in the catalytic flow reactor. Further increases in mass flow rate were limited not by reactivity but by the flow supply system. Note that there exists an equivalence ratio under which the catalyst performs poorly; in the flow reactor, 0.5 may be argued to be this equivalence ratio. The reason for this limit is yet to be discovered. More importantly, the exhaust gas temperature is lower compared with that from the gas-phase results, while the structural temperature is higher. This is because the reactions take place on the catalyst surface, not in the gas stream. The heat released from the reactions tends to flow into the structure due to the existence of a short conduction path rather than into the gas by convection. To summarize, the gas-phase micro-combustor satisfied the exhaust gas temperature requirement, whereas it did not meet the mass flow rate capability. In contrast, the results from the catalytic flow reactor show that the catalytic micro-combustor may have mass flow rate capability to meet the design requirement, but may not satisfy the exhaust gas temperature requirement. Spadaccini has suggested that catalytic combustion in the micro-combustor appears to be a diffusion-controlled process [14]. The results in the catalytic flow reactor are supporting this argument. If that is the case, increasing the surface area of the catalytic insert will be one possible solution to improve efficiency, as long as the denser insert does not violate the total pressure loss requirement. The total pressure loss across the combustion chamber is

less than 1% as shown in Figure 3.3. This indicates that the density of inserts can be increased without exceeding the requirement of 5%. Using denser inserts will be further discussed in Section 3.3.

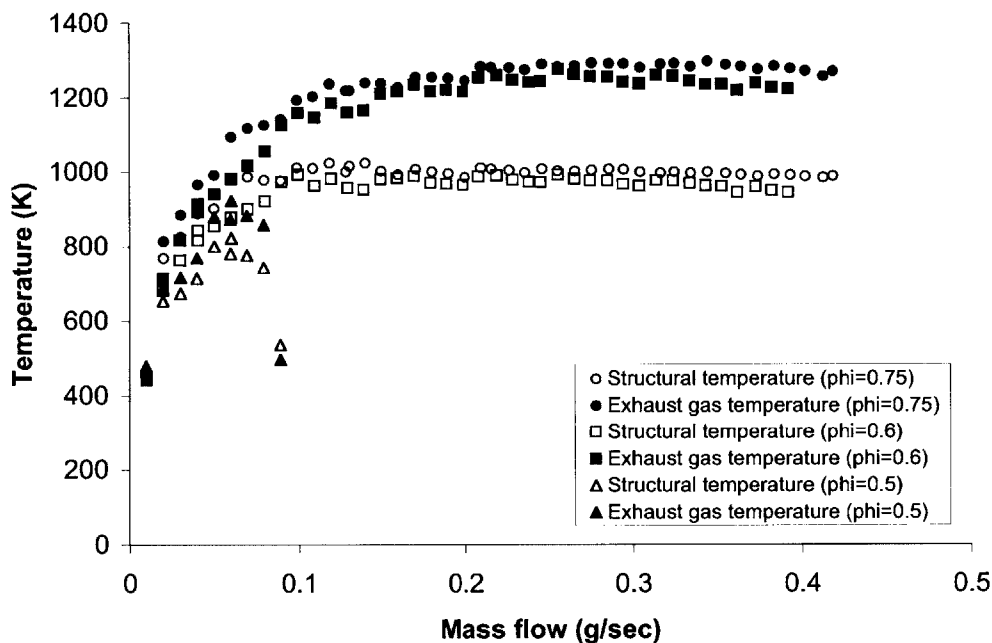


Figure 3.1: Results of catalytic propane/air combustion over platinum insert

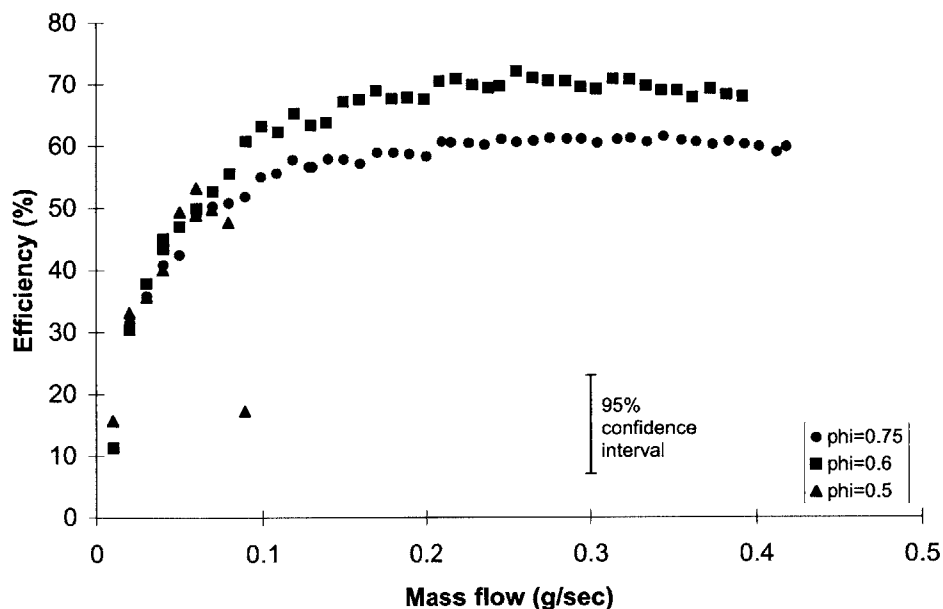


Figure 3.2: Combustor efficiency for catalytic propane/air combustion over platinum insert

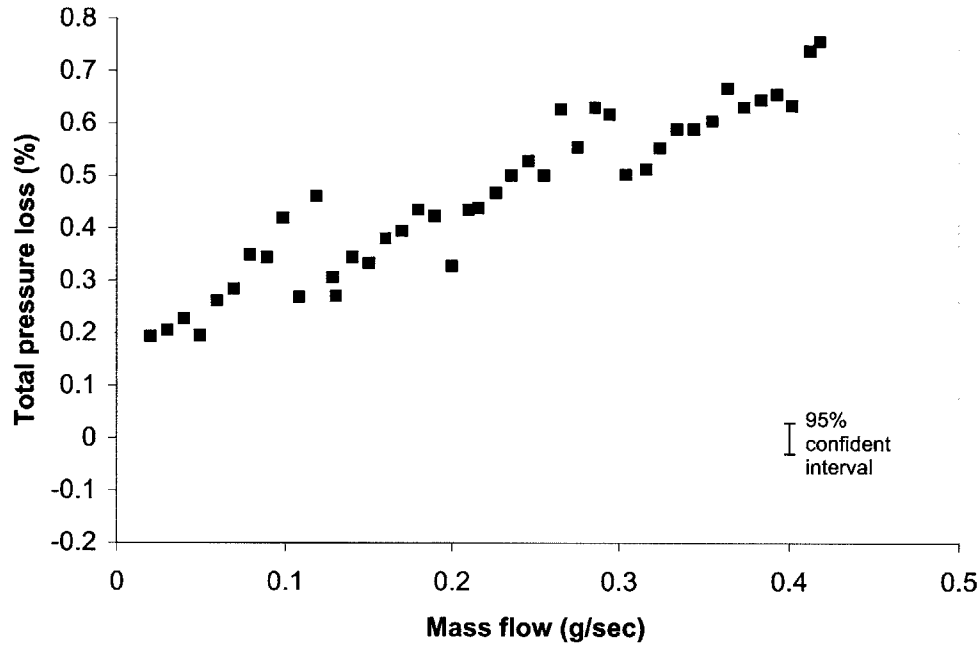


Figure 3.3: Total pressure loss across combustion chamber for catalytic propane/air combustion with equivalence ratio 0.75

3.2 CATALYTIC IGNITION AND EXTINCTION TEST USING HYDROGEN

It is known that the surface temperature of the catalyst must reach a threshold temperature to ignite heterogeneous surface reactions. For example, as a hydrogen/air mixture is passed over a piece of platinum, which is heated resistively, there will be a sudden temperature rise indicating ignition. On the other hand, as the electrical power going into the platinum piece is decreased, the reaction is finally extinguished at a temperature lower than where it lit off [17]. This ignition and extinction hysteresis is common in catalytic systems.

To see if this hysteresis can be observed in the catalytic micro-combustor, catalytic ignition and extinction tests using hydrogen were conducted in the flow reactor. Instead of using resistive heating, the external heater that has been used to control the wall temperature was utilized. A hydrogen/air mixture with equivalence ratio of 0.4 and mass flow rate of 0.03g/sec was introduced through the flow reactor while adjusting the heater setting. As shown in Figure 3.4, temperatures responded to the heater setting at

low settings. When the heater setting reached 30%, a sudden rise in temperature was observed. This is because the mixture lights off over the platinum surface. Then, the temperatures followed the heater setting well again after the ignition. It was tested up to 40% before reducing the heater setting. As the heater power was reduced, the temperatures responded well without showing any sign of extinction all the way down to zero, i.e. the catalytic combustion was self-sustained, or auto-thermal

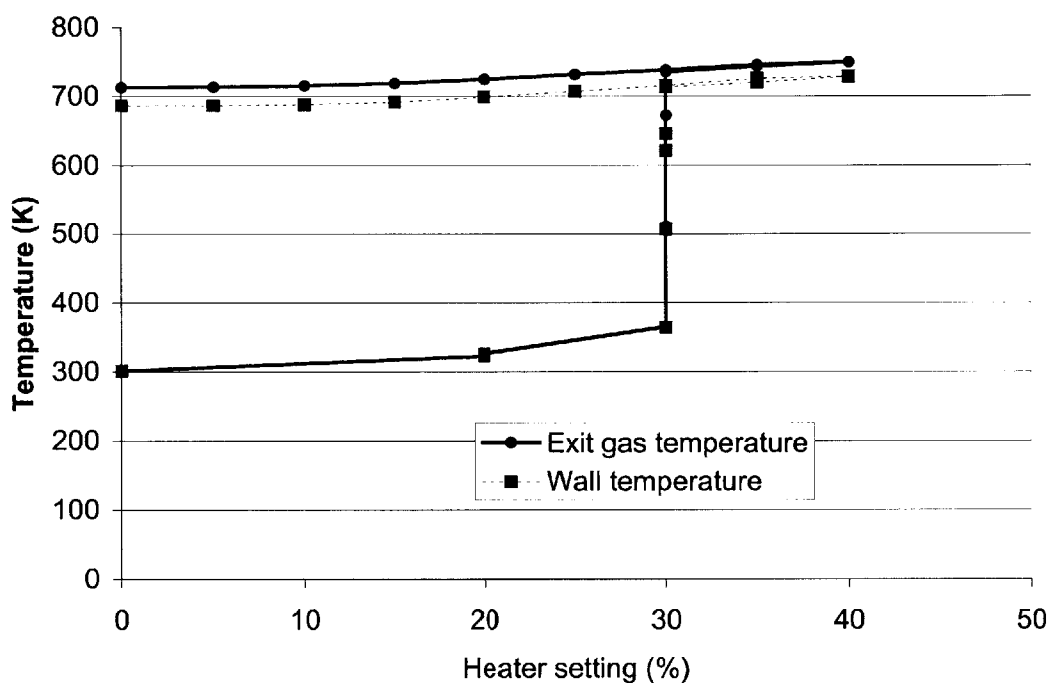


Figure 3.4: Catalytic ignition and extinction hysteresis

3.3 CATALYTIC COMBUSTION OVER A DENSER CATALYTIC INSERT

3.3.1 Motivation

Analyses and experiments to date suggest that the combustion process of propane in the catalytic micro-combustor appears to be a diffusion-controlled [14]. In other words, chemical reactions of propane and air are fast enough not to limit the process, but the diffusion of propane to the surface is slow and pacing the process. If this is the case, increasing the surface area would help chemical efficiencies increase.

3.3.2 Procedure

Therefore, as a preliminary exploration of denser materials, two inserts squeezed down by half of their thickness were put together into the combustion chamber. This will roughly double the density of the foam and the surface area. The porosity becomes approximately 88%.

3.3.3 Results

Figures 3.5 and 3.6 show the results of using the double-density foam, and shown in Figure 3.7 is the temperature response for the single-density foam and double-density foam experiments plotted on one chart. In general, the results do not look very different from those with the single-density foam. However, the results for equivalence ratio 0.75 seem to deviate from the results for the single-density foam tests. A little enhancement in the exhaust gas temperature was achieved, but the structure gained much more temperature as shown in Figure 3.7. This implies that although chemical efficiency can be improved by denser foam, thermal efficiency may become lower unless good thermal insulation is applied, resulting in little improvement in overall combustor efficiency. The efficiency analysis will be presented in Chapter 4 in more detail. In addition, the total pressure loss still remained within 2% even with the double-density insert as shown in Figure 3.8. The experimental results qualitatively agree with the reduced order modeling that can be found in the Spadaccini [14].

3.4 INSPECTION OF USED CATALYTIC INSERTS

After hours of testing, no significant damage was visible in the inserts except a dulling in color. In order to investigate possible material degradation during combustion, the inserts were inspected under a scanning electron microscope (or SEM). The pure nickel surface looked quite bumpy itself as shown in Figure 3.9, but after impregnating platinum, the surface became smooth indicating that platinum is covering most of the surface.

However, some peeling is observable in Figure 3.10. After testing, the peeling is more pronounced, and the surface becomes rougher as shown in Figure 3.11. Efforts to draw additional information from the SEM images are continuing. Further, more systematic characterization of catalytic material is on-going.

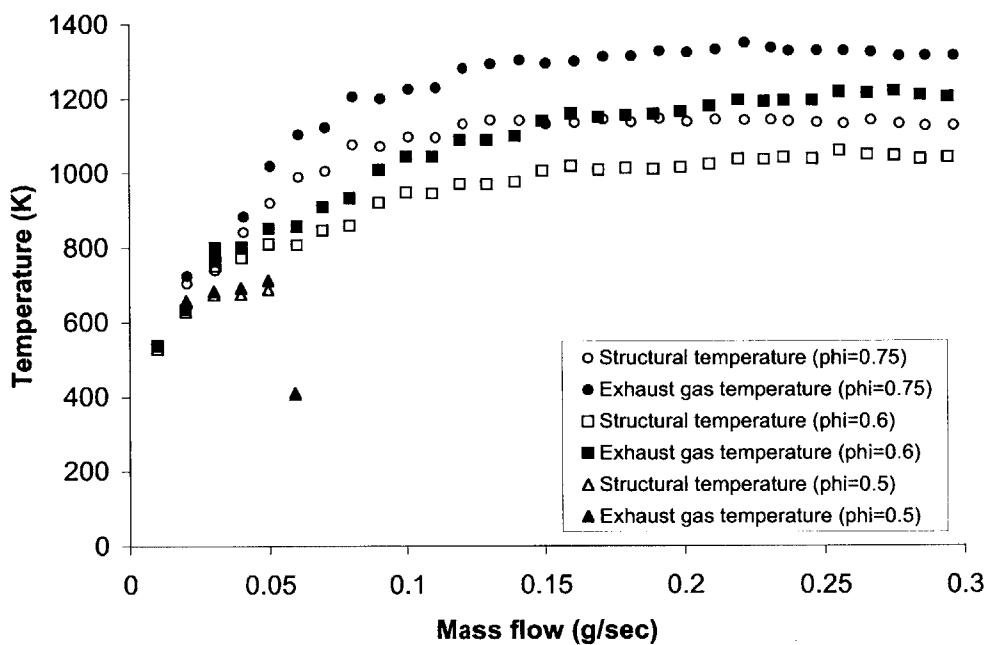


Figure 3.5: Results of catalytic propane/air combustion over double-density platinum insert

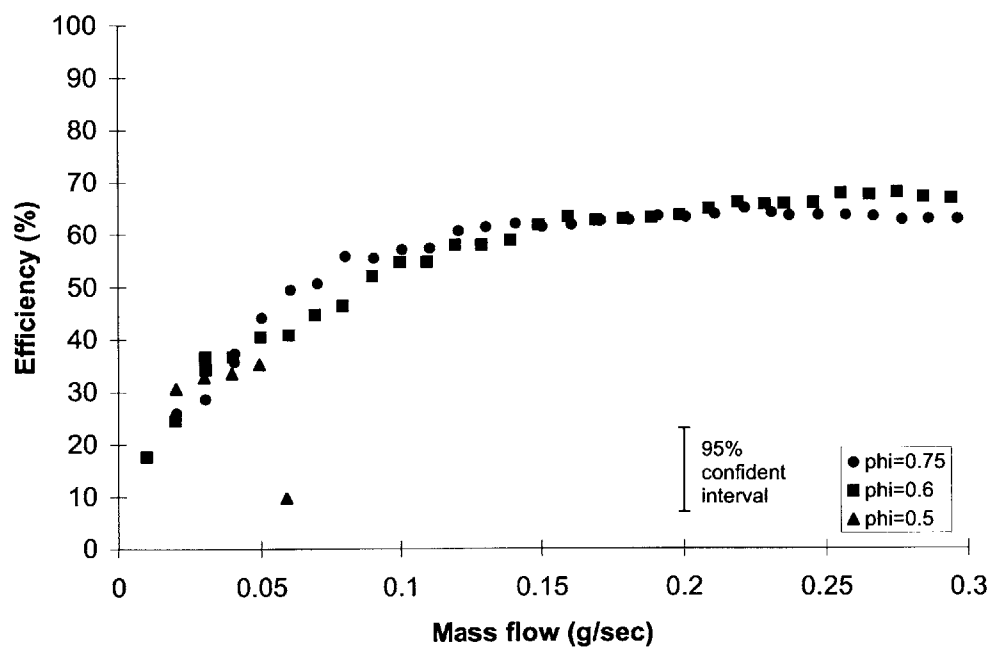


Figure 3.6: Combustor efficiency for catalytic propane/air combustion over double-density platinum insert

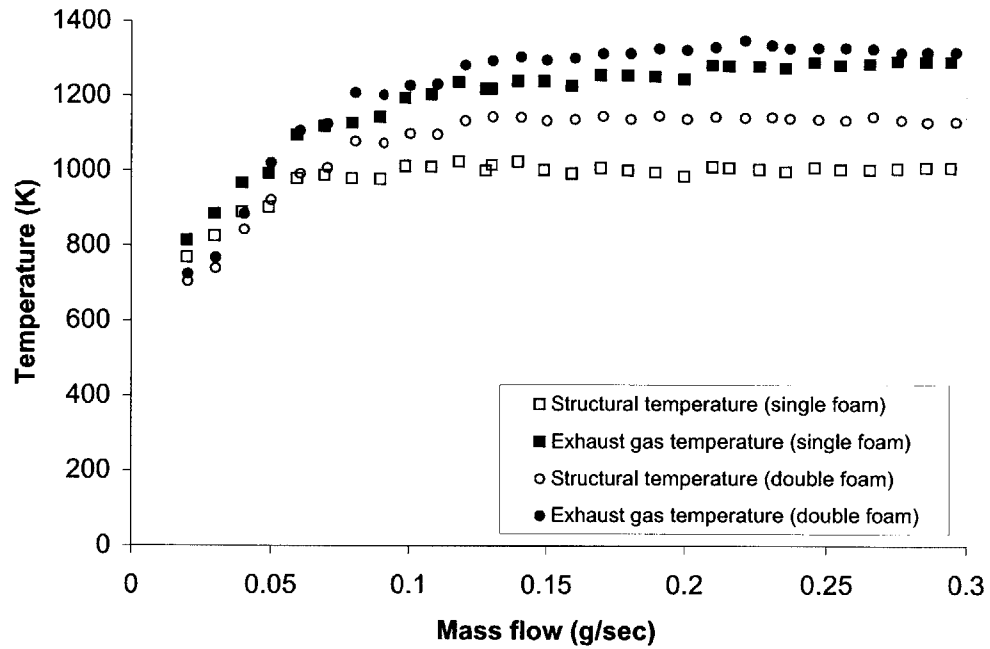


Figure 3.7: Comparison of temperature response for single-density and double-density foam experiments (propane, $\phi=0.75$)

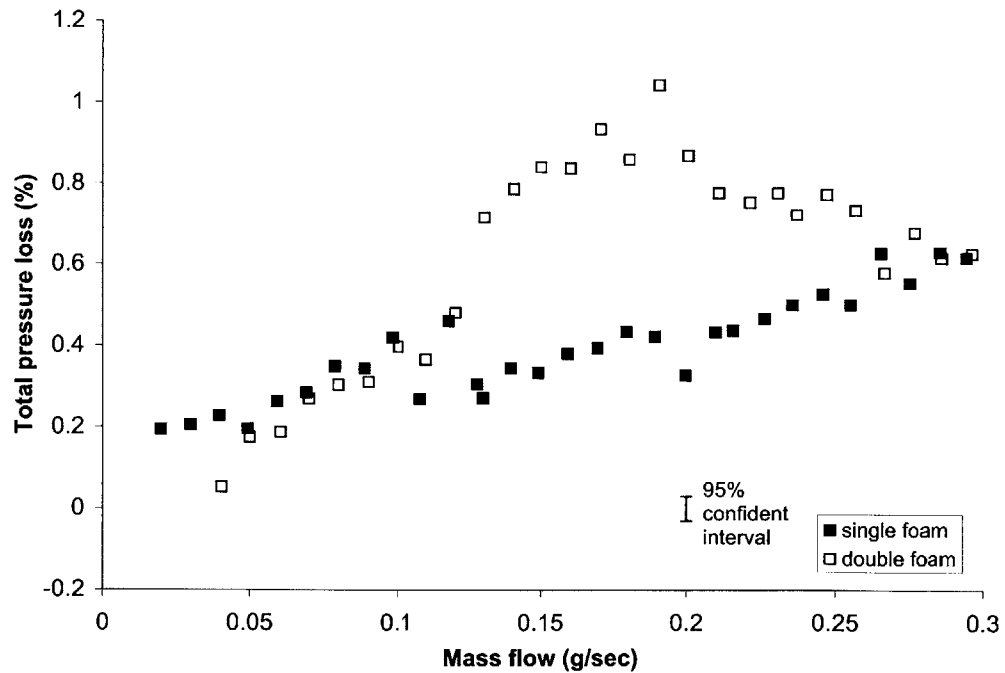


Figure 3.8: Comparison of total pressure loss for single-density and double-density foam experiments (propane, $\phi=0.75$)

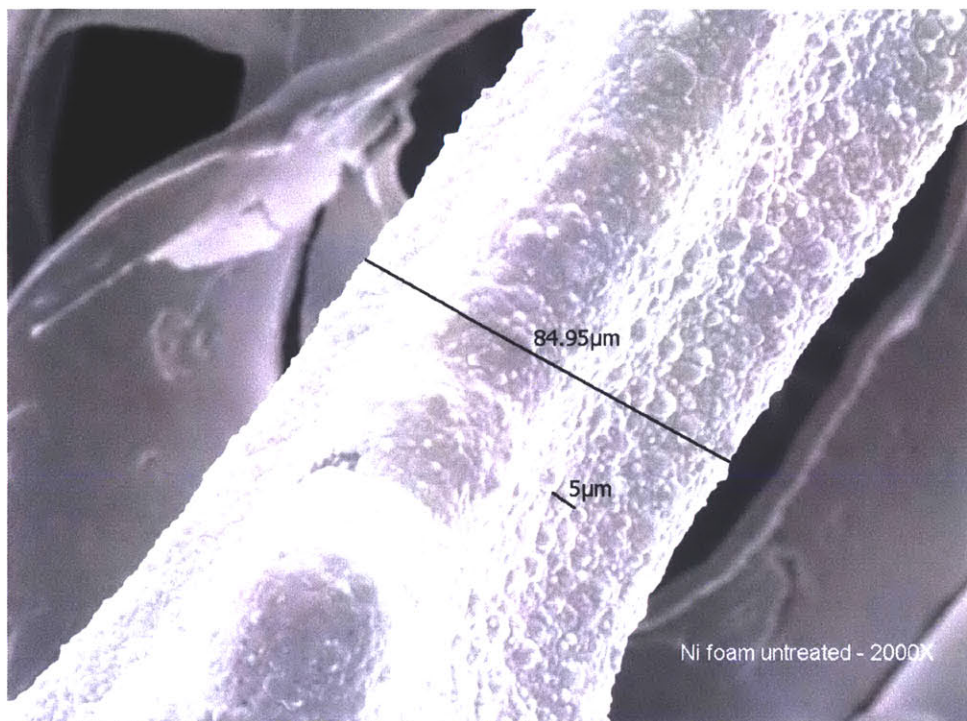


Figure 3.9: SEM of untreated nickel insert

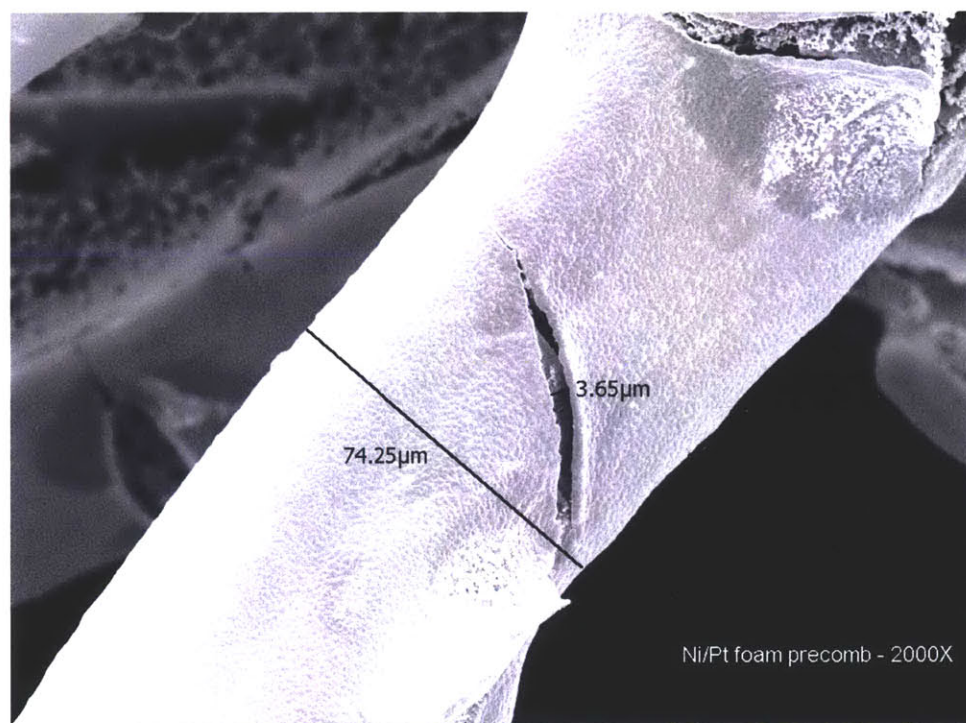
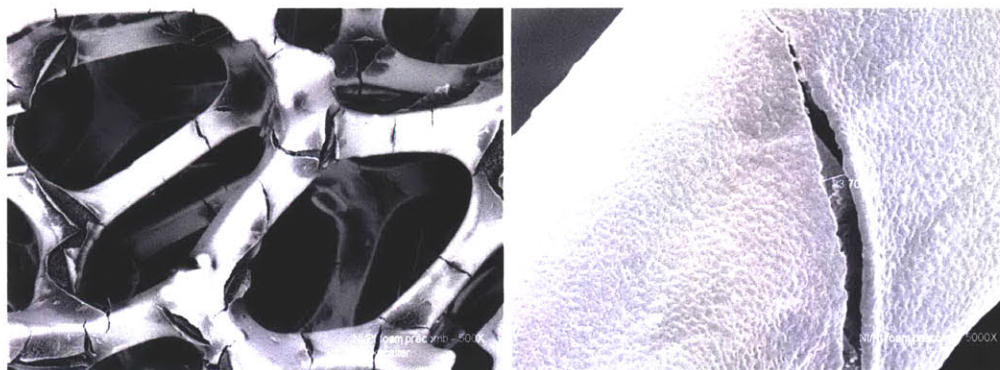


Figure 3.10: SEM's of platinum (coated on nickel) insert before testing

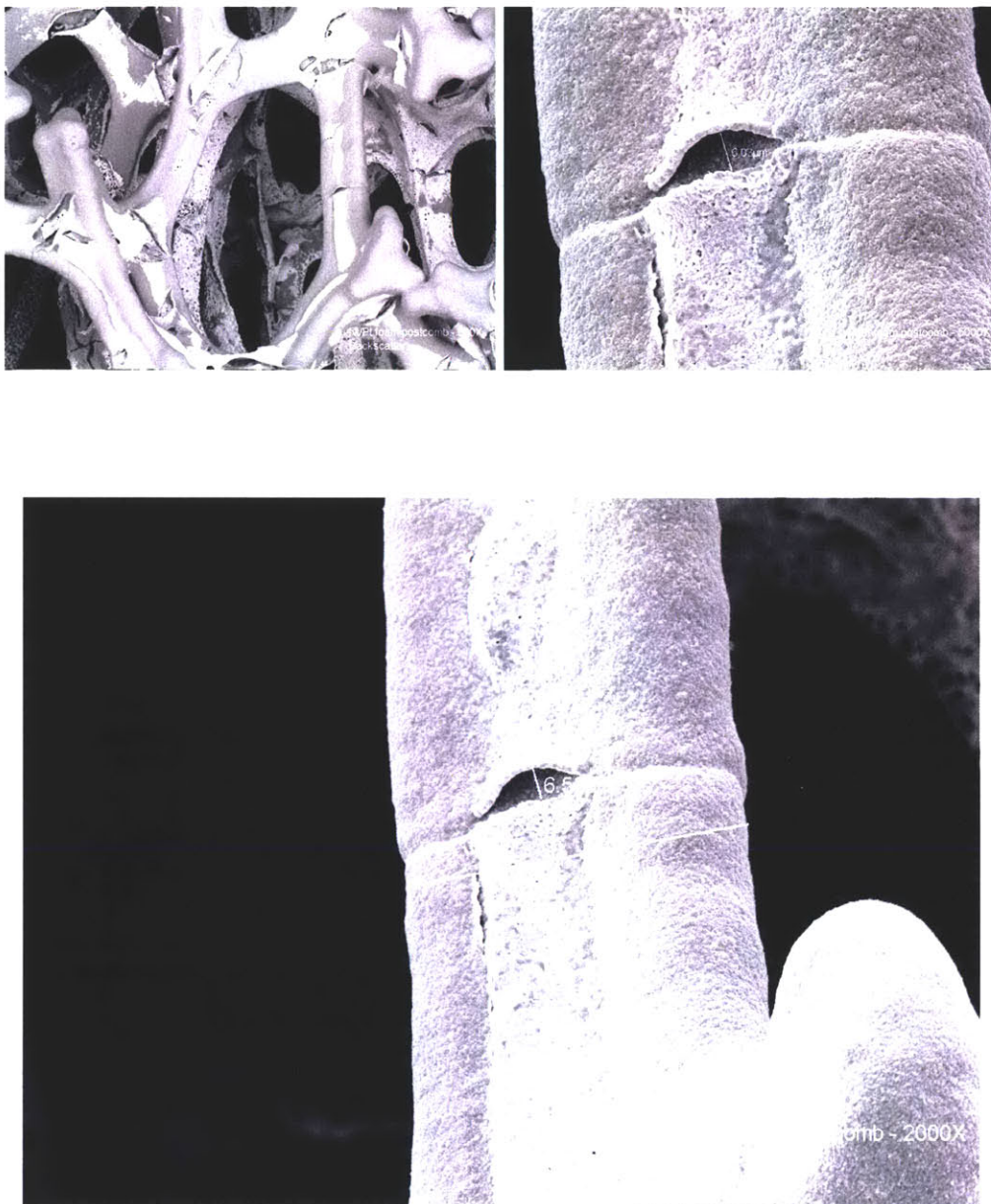


Figure 3.11: SEM's of platinum insert after testing

3.5 CHAPTER SUMMARY

Using the conventionally-machined catalytic flow reactor described in Chapter 2, catalytic propane/air combustion was achieved. This was done by following a catalytic ignition procedure converting the fuel gradually from hydrogen to propane. Upon accomplishing catalytic propane/air combustion in the micro-combustor geometry, there was significant enhancement of mass flow rate capability, so that the design requirement was met. However, low exhaust gas temperature was a new issue. In an attempt to

address this issue, a denser catalytic insert was proposed and tested in the flow reactor. Initial results were that denser foam does improve the performance.

A hysteresis diagram of catalytic ignition and extinction of hydrogen/air was obtained showing the behavior of the catalytic reaction in the flow reactor is consistent with similar results reported in the literature.

After testing, the catalytic inserts were examined under a scanning electron microscope, and compared with untested inserts. The coated platinum seemed quite viable through hours of combustion. More detailed analyses of the surface, e.g. surface area measurement, surface composition analysis, etc., are scheduled to be performed.

CHAPTER 4

NUMERICAL MODELING RESULTS

4.1 NUMERICAL TOOLS

The objective of developing a finite element heat transfer model is to characterize the catalytic micro-combustor without intensive calculation. For this reason, a fluid/structure interaction model [7] that is computationally expensive was not pursued. ABAQUS was recommended for this purpose [11].

4.1.1 ABAQUS

ABAQUS is a commercial software package for finite element analysis. It is known to be a powerful and reliable solver for linear and nonlinear engineering problems using finite element methods. A wide range of structural, thermal, and coupled analyses are supported. For the present research, version 6.3 was used [1].

4.1.2 PATRAN

Although ABAQUS is a powerful tool, its text-based interface is difficult to use. A user provides an input script containing all the geometric and element information, boundary conditions, and material properties. This usually becomes intensive, as the geometry gets complex. PATRAN was originally developed as a pre-processor to NASTRAN, another powerful finite element analysis tool. Now PATRAN itself has become a general-purpose finite element mesh generator that can generate input files for several different finite element codes including ABAQUS. It can perform certain post-processing jobs as

well. Thanks to its graphical and intuitive user-interface, PATRAN was used when generating the input scripts to ABAQUS for the present research.

4.2 CALCULATION PROCEDURE

4.2.1 Geometry and Grid Generation

Using PATRAN, geometries representing both the micro-combustor and the catalytic flow reactor were generated based on actual dimensions. The micro-combustor and the flow reactor were modeled as axi-symmetric. Any parts that are not axi-symmetric were replaced by equivalent axi-symmetric geometries by reducing the coefficient of thermal conductivity according to the area ratio. One example of the equivalent axi-symmetric geometry is shown in Figure 4.1.

Grid systems were also generated using PATRAN. For the sake of simplicity, rectangular elements were used.

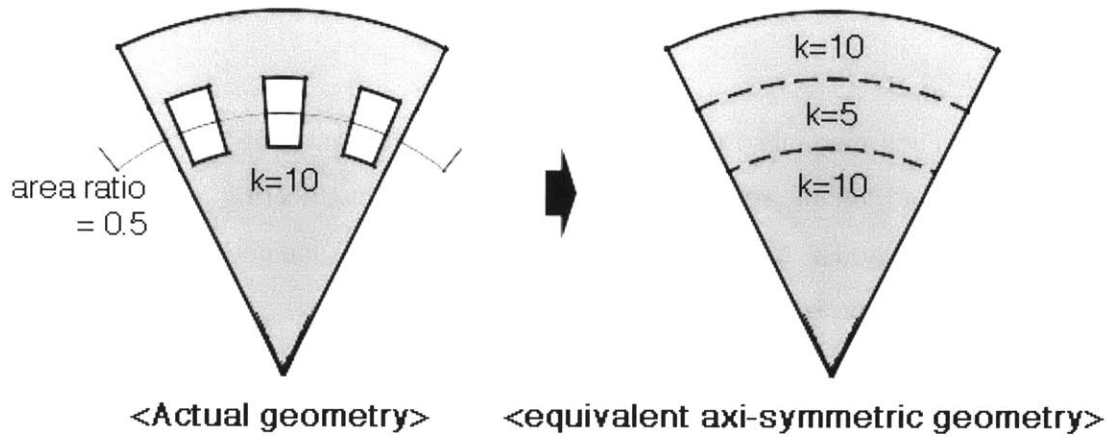


Figure 4.1: Replacement of non-axi-symmetric geometry

4.2.2 Boundary Conditions

A natural convection boundary condition was used on the exterior, wall ③ in Figure 4.2. Incropera and De Witt suggested $25\text{W/m}^2\text{K}$ as the heat transfer coefficient of the natural convection [6], which was adopted for the present calculation. Wall ① is where the incoming flow is impinged before it makes a right angle turn. In calculating the heat transfer coefficient of an impinging jet, Equations 4.1, 4.2, 4.3, and 4.4 can be used. In

Equations 4.2 and 4.3, F_1 and G are obtained using the Reynolds number along with geometric information. The Nusselt number is then calculated from above-obtained F_1 , G and the corresponding Prandtl number. Finally, the overall heat transfer coefficient h is calculated.

$$\frac{Nu}{Pr^{0.42}} = GF_1 \quad \text{<Eq. 4.1>}$$

where,

$$F_1 = 2Re^{1/2}(1 + 0.005Re^{0.55})^{1/2} \quad \text{<Eq. 4.2>}$$

$$G = \frac{D}{r} \frac{1 - 1.1D/r}{1 + 0.1(H/D - 6)D/r} \quad \text{<Eq. 4.3>}$$

$$h = \frac{Nu \ k}{L} \quad \text{<Eq. 4.4>}$$

The boundary conditions at walls ② and ④ were set as convection in circular tubes. The Nusselt number was estimated as 15 from empirical correlations. Then the overall heat transfer coefficient was obtained using Equation 4.4 again.

Wall ⑥ is the centerline of axial symmetry. Thus, an adiabatic condition is appropriate. All the other walls such as those of the recirculation jacket and wall ⑤ were also assumed to be adiabatic. The overall heat transfer coefficients on each wall are listed in Table 4.1.

Table 4.1: Overall heat transfer coefficients on each wall of micro-combustor geometry

Wall	Condition	Approx. gas temp.	h [W/m ² K]
1	Impinging jet	300K	772
2	Circular tube	300K	98.6
3	Natural convection	300K	25
4	Circular tube	1500K	202.7
5	Adiabatic	1500K	0
6	Adiabatic	N/A	0

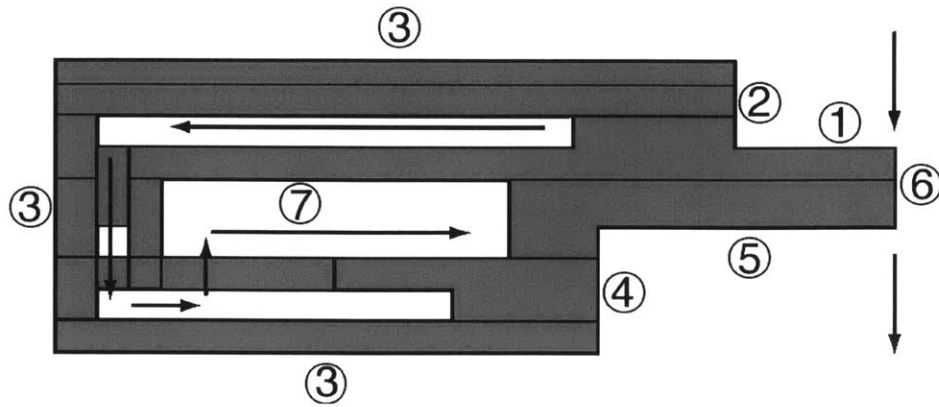


Figure 4.2: Station numbering on micro-combustor geometry showing flow path

4.2.3 Calculation Procedure

In order to run ABAQUS, grid systems corresponding both to the micro-combustor geometry and to the catalytic flow reactor geometry were generated using PATRAN. All the boundary conditions were implemented through PATRAN as well. Input was the total heat dissipated through the structure. To do this, a uniformly distributed heat flux was set along the inner combustion chamber wall (wall ⑦ in Figure 4.2). For a uniform heat flux across the combustion chamber wall, in addition to the boundary conditions listed in Table 4.1, ABAQUS calculates the temperature profile throughout the structure. Looking at the results, one checks the calculated temperature at the location in the geometry where it is measured experimentally, and compares the two results. Only a single value of heat flux value makes the measured and calculated temperatures match. This value is found by trial and error. The temperature profile obtained is the temperature profile for that particular case of the experiment. The result can then be used to evaluate the chemical, thermal, and combustor efficiencies. Integrating this unique heat flux value along the combustion chamber wall, the total heat dissipated through the structure is calculated for each case of the experiment. The enthalpy rise of the gas from the inlet to the exit can be calculated since the exhaust gas temperature and the inlet temperature are measured. The summation of the heats dissipated through the structure and gained by the gas becomes the total heat generated during the combustion process. The fraction of this total heat generation to the total energy that the fuel contains is the chemical efficiency. The ratio of the heat gained by the gas to the total heat generation is

the thermal efficiency. The ratio of the heat that is retained in the gas to the energy of the fuel (the enthalpy of formation) becomes the overall combustor efficiency. The product of the chemical efficiency and the thermal efficiency is the combustor efficiency. The definitions of the efficiencies are given in Equations 4.5, 4.6, and 4.7 [10]:

$$\eta_{chem} = \frac{[(\dot{m}_a + \dot{m}_f)h_2 - \dot{m}_a h_1] + \dot{Q}_{loss}}{\dot{m}_f h_f} \quad <Eq. 4.5>$$

$$\eta_{thermal} = \frac{(\dot{m}_a + \dot{m}_f)h_2 - \dot{m}_a h_1}{[(\dot{m}_a + \dot{m}_f)h_2 - \dot{m}_a h_1] + \dot{Q}_{loss}} \quad <Eq. 4.6>$$

$$\eta_{combustor} = \frac{(\dot{m}_a + \dot{m}_f)h_2 - \dot{m}_a h_1}{\dot{m}_f h_f} = \eta_{chem} \times \eta_{thermal} \quad <Eq. 4.7>$$

4.2.4 Validation of the Model

To check the validity of the finite element heat transfer model, several assessments were made. First, a grid refinement study was performed. The same calculation was done for a much denser grid and for a much coarser grid. They all yielded nearly the same temperature profile. Second, the catalytic flow reactor with improved measurement accessibility was used to verify that the temperature profile calculated by the finite element model matched experimental measurements. Shown in Figure 4.3 is a sample case for the flow reactor geometry. The table below the figure indicates that the measured temperatures and calculated temperatures agree well. Circumferential uniformity was also checked in the catalytic flow reactor, and found to be acceptable. It supports the validity of assuming axi-symmetry.

4.3 MICRO-COMBUSTOR RESULTS

4.3.1 Temperature Distribution

Following the procedure described in 4.2.3, the temperature profile in the micro-combustor was obtained. Figure 4.4 shows a typical result. As expected, the temperature difference between the hottest spot and the coldest is not significant; the structure is

nearly isothermal. This is because the thermal conductivity of silicon is relatively high, and conduction is not the limiting heat transfer mechanism in the micro-combustor.

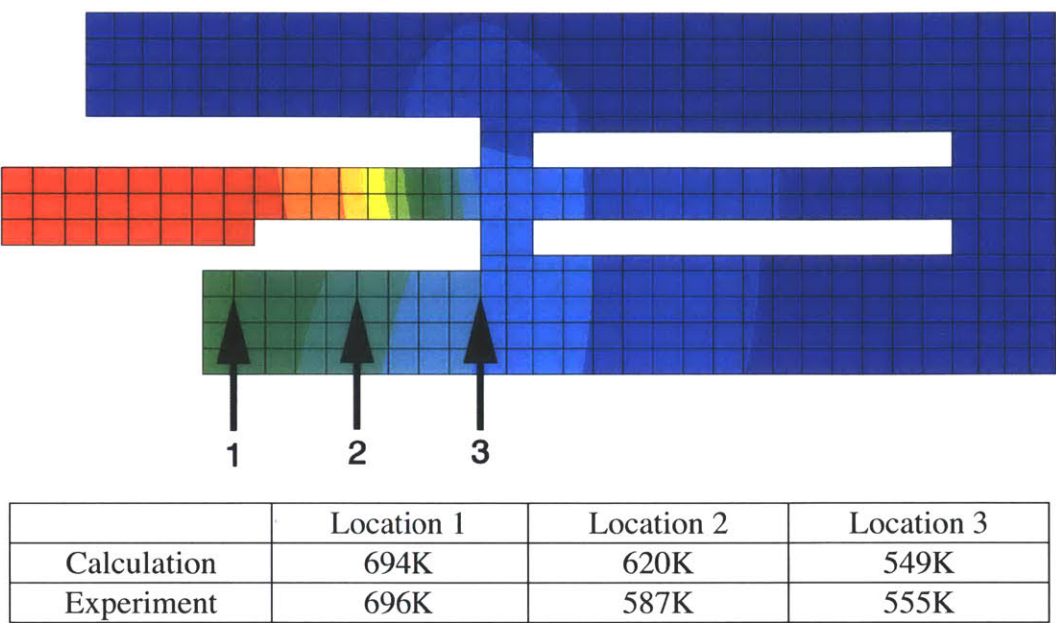


Figure 4.3: Experimental validation of finite element heat transfer model

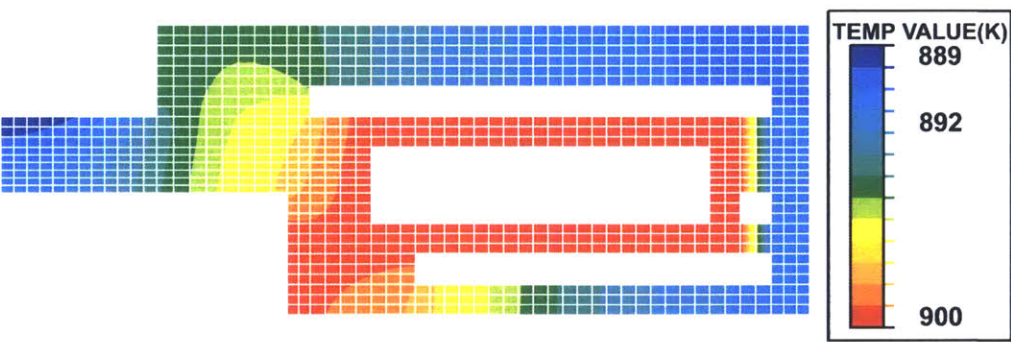


Figure 4.4: Temperature profile calculated by finite element heat transfer model for micro-combustor geometry

4.3.2 Efficiency Breakdown

The overall combustor efficiency was broken down into the chemical and the thermal efficiencies as stated in 4.2.3. In Figure 4.5, square symbols represent thermal

efficiencies obtained with the finite element model, and dot symbols represent chemical efficiencies. The experimental data are from the Mehra [10], and efficiencies were estimated using a 1-D heat transfer model. For a 1-D model to be valid, the structure must be nearly isothermal. The finite element heat transfer model corroborated that the structure is approximately isothermal, and the efficiency components estimated by Mehra and the FEM model matched well.

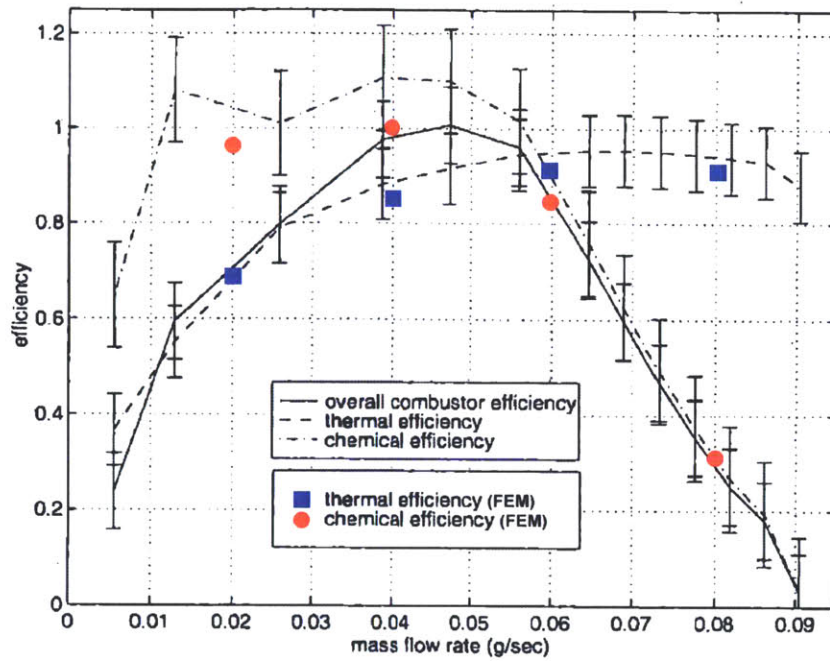


Figure 4.5: Efficiency breakdown for micro-combustor (hydrogen, $\phi=0.4$)

4.4 CATALYTIC FLOW REACTOR RESULTS

4.4.1 Temperature Distribution

A similar calculation was conducted for the catalytic flow reactor geometry. All the boundary conditions and the calculation procedure were the same as those for the micro-combustor geometry except for the gaskets. It was assumed that there was no heat flux between the gaskets and the Macor® structure. Shown in Figure 4.6 is a typical temperature distribution for the flow reactor geometry. It can be seen that it has a much larger temperature gradient due to the low thermal conductivity of Macor®, compared to silicon.

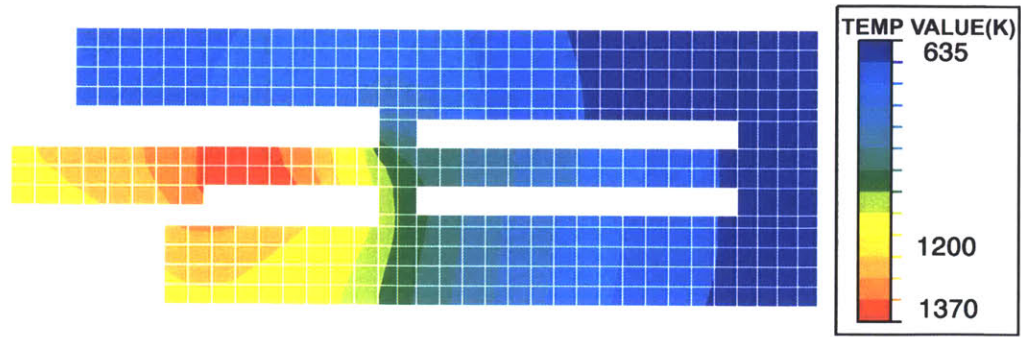


Figure 4.6: Temperature profile calculated by finite element heat transfer model for catalytic flow reactor geometry

4.4.2 Efficiency Breakdown

A similar procedure to the one used for the micro-combustor was repeated to break the overall combustor efficiency into the chemical and the thermal efficiencies. Due to the large temperature gradient in the structure, a one-dimensional heat transfer analysis similar to that used for the micro-combustor would not work. The efficiency breakdown was made possible only by the finite element heat transfer model.

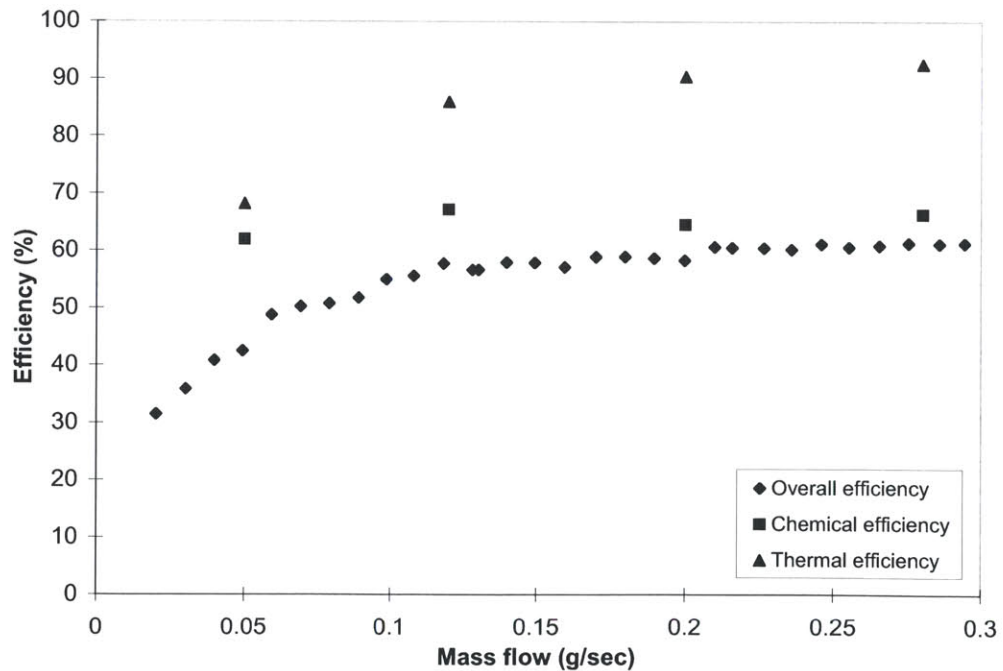


Figure 4.7: Efficiency breakdown for catalytic flow reactor (propane, $\phi=0.75$)

4.5 COMPARISON OF SINGLE-DENSITY AND DOUBLE-DENSITY FOAM

The overall efficiency obtained from the double-density insert experiment mentioned in 3.4 was broken down into the thermal and the chemical efficiencies, and compared with those from the single-density insert. In Figure 4.8, note that the overall combustor efficiency does not increase much by using a denser insert, whereas the chemical efficiency does. This is due to the reduction in the thermal efficiency. Because of the higher structural temperature, more heat was lost from the device instead of being retained in the gas. Therefore, the next generation catalytic micro-combustor may require improved thermal insulation between the catalytic foam and the silicon structure.

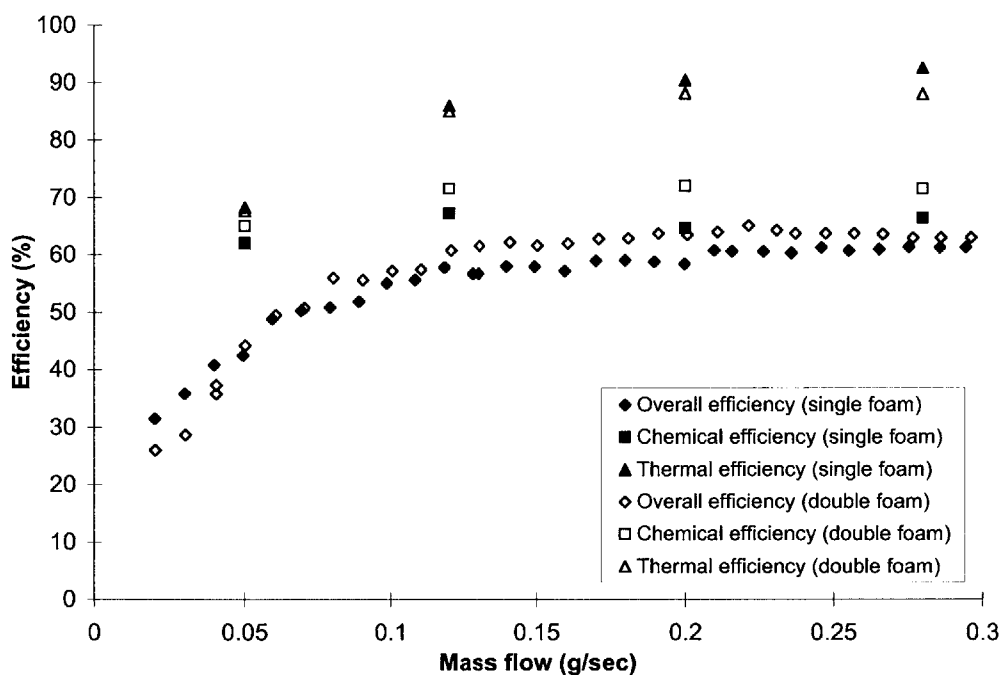


Figure 4.8: Comparison of efficiencies for single-density foam and double-density foam (propane, $\phi=0.75$)

4.6 CHAPTER SUMMARY

Utilizing a commercially available finite element analysis package, ABAQUS, a 3-D heat transfer analysis was performed both for the micro-combustor geometry and for the catalytic flow reactor geometry. By doing this, more accurate estimation of the chemical

and thermal efficiencies was possible. For the micro-combustor geometry, the structure was nearly isothermal due to the high thermal conductivity. In contrast, there exists a large temperature gradient in the catalytic flow reactor due to the low thermal conductivity of Macor®. Consequently, the finite element model is vital in estimating the chemical and thermal efficiencies in the flow reactor. The efficiency breakdown for the double-density insert experiment indicates that a denser insert does increase the fraction of chemical conversion, although larger thermal loss undermines the advantage.

CHAPTER 5

CONCLUSIONS

5.1 SUMMARY OF THE EXPERIMENTS AND ANALYSES

Previous research explored the feasibility of burning homogeneous gas-phase hydrocarbons in the micro-combustor, but without much success. Gas-phase micro-combustors were able to achieve the exhaust gas temperature requirement, but failed to meet the mass flow rate requirement. As a potential improvement, heterogeneous catalytic combustion was proposed. To evaluate catalyst operability, a catalytic flow reactor was built without the micro-fabrication techniques. Auto-thermal catalytic propane/air combustion was stabilized in the same geometry and scale as the micro-combustor for the first time. The mass flow rate requirement was met, but the exhaust gas temperature was too low to satisfy the design requirement. Spadaccini has concluded that the catalytic combustion process is controlled by the diffusion of fuel to the catalyst surface [14]. As long as it is diffusion controlled, the type of catalyst would not make much difference. Rather, using denser foam would be able to improve the performance. To validate this idea, double-density platinum foam was tested in the flow reactor. The conversion rate of fuel increased by using denser foam. However, the finite element heat transfer model that was discussed in Chapter 4 indicated that even if the conversion rate of fuel increases, the combustor efficiency itself may not increase to a desired level, unless the design of the catalytic micro-combustor manages the heat loss effectively.

5.2 DESIGN SUGGESTIONS FOR THE SECOND GENERATION CATALYTIC MICRO-COMBUSTOR

Experiments and modeling efforts to date draw the following design suggestions for the next generation catalytic micro-combustor.

- (1) Using a catalytic insert as dense as the total pressure loss requirement allows will be helpful in increasing the chemical efficiency.
- (2) For a better heat loss management, a improved thermal insulation between the catalytic insert and the silicon structure may be required.
- (3) If a better heat loss management scheme is implemented, thermal durability of the insert may become an issue. Investigation of inserts that are more thermally durable should be conducted.
- (4) Since conversion from one fuel to another to ignite catalytic combustion is not practical, a better catalytic ignition scheme should be pursued.

5.3 CONTINUING WORK

The second generation catalytic micro-combustor is being fabricated currently. It has the same geometry as the first generation catalytic micro-combustor. The only difference will be the catalytic inserts put inside the combustion chamber. Platinum is still the catalytic material of choice for the next generation catalytic micro-combustor. The differences will include,

- (1) The type of support materials: desire for a better thermal durability
- (2) The coating method of platinum on the support: desire for better thermal durability
- (3) The density of catalytic inserts: to systematically examine the effect of the density of the inserts

Several different metal foams such as Inconel and FeCrAlY were obtained. Some of them are coated with platinum by dipping in platinum solution and drying, while others are treated by platinum ionic plasma impregnation. The porosity of the foam ranges from 78% to 92%. Characterization of the inserts is also underway. This includes SEM imaging, surface area measurements, and composition analysis.

5.4 RECOMMENDATIONS FOR FUTURE WORK

In the short-term, the catalytic micro-combustor research will be focusing primarily on fabricating and testing the design guidelines suggested in the present thesis. The catalytic inserts being prepared are to be inserted into the silicon structure. After bonding and packaging is done, the second generation catalytic micro-combustors will be tested and analyzed. Issues of interest will be:

- (1) Whether denser foam increases the chemical efficiency as it did in the catalytic flow reactor.
- (2) What different support materials and treatment methods do to the thermal durability of the inserts

As longer-term issues, the catalytic ignition scheme will be revised, and a method for a better thermal insulation of the catalytic insert will be pursued. Feasibility of using heavier fuels such as JP8 and kerosene will be evaluated as well.

APPENDIX A

DRAWINGS OF CATALYTIC FLOW REACTOR

A.1 TOP-PLATE

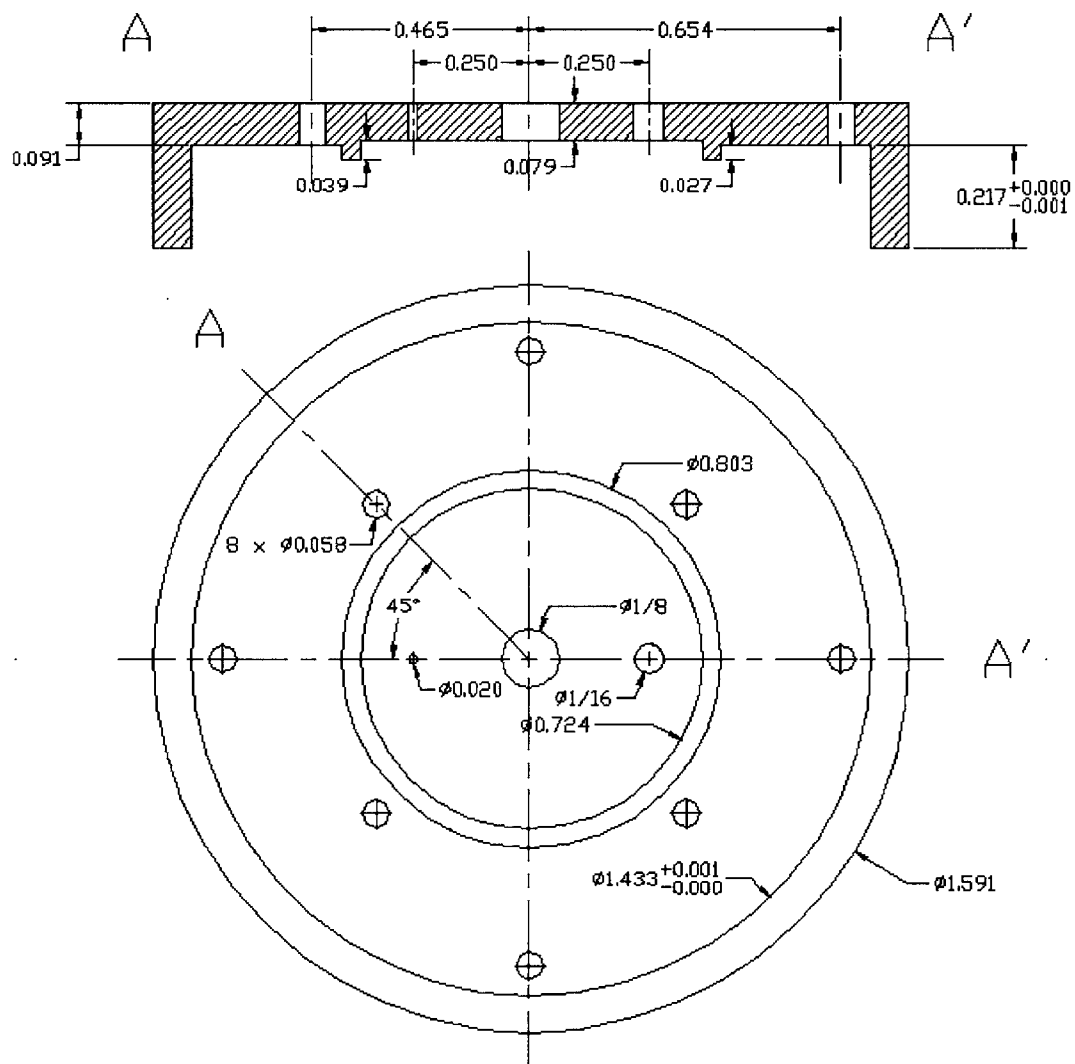


Figure A.1: Mechanical drawing of the top-plate of the catalytic flow reactor

A.2 MIDDLE-PLATE

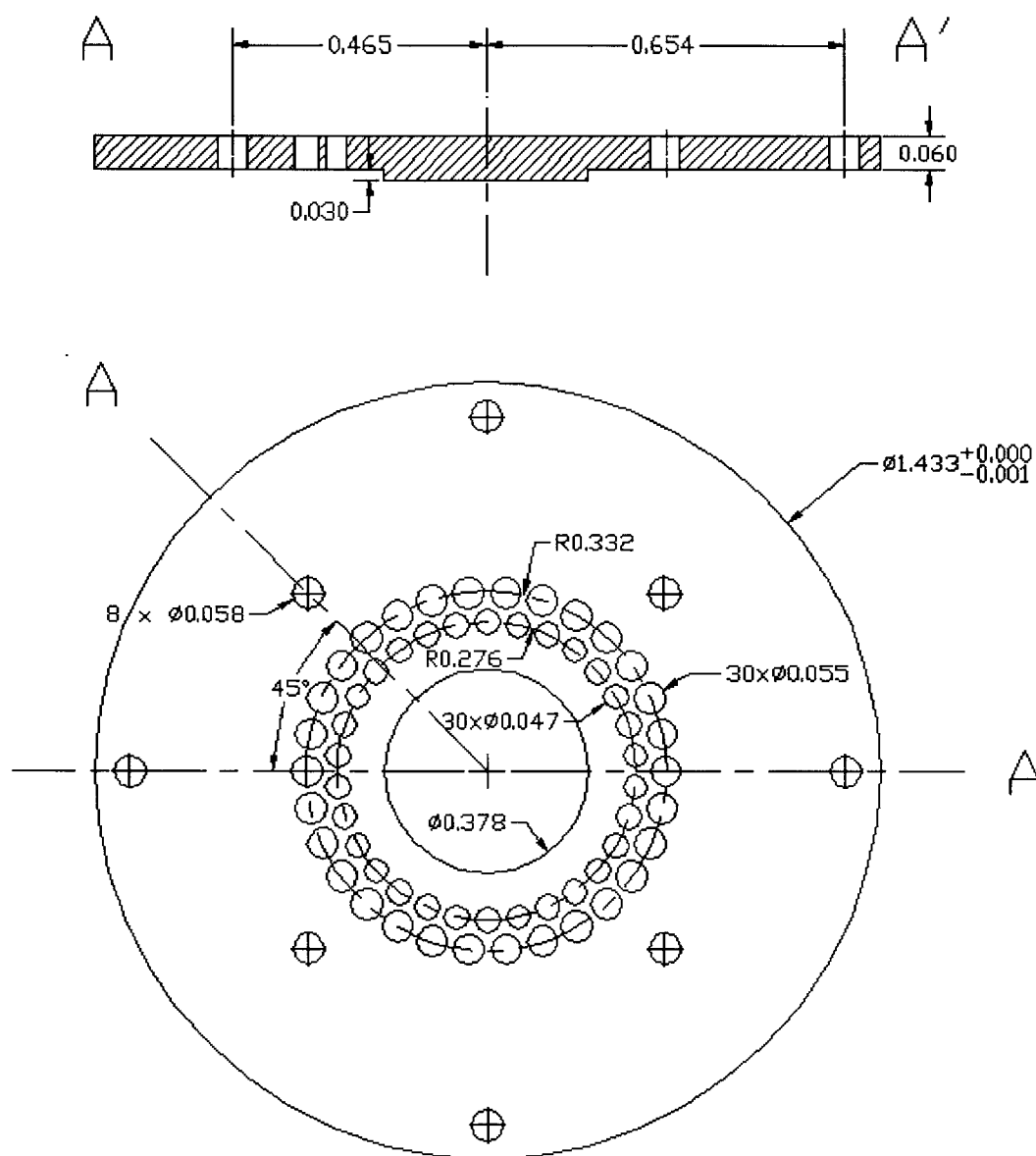


Figure A.2: Mechanical drawing of the middle-plate of the catalytic flow reactor

A.3 BOTTOM-PLATE

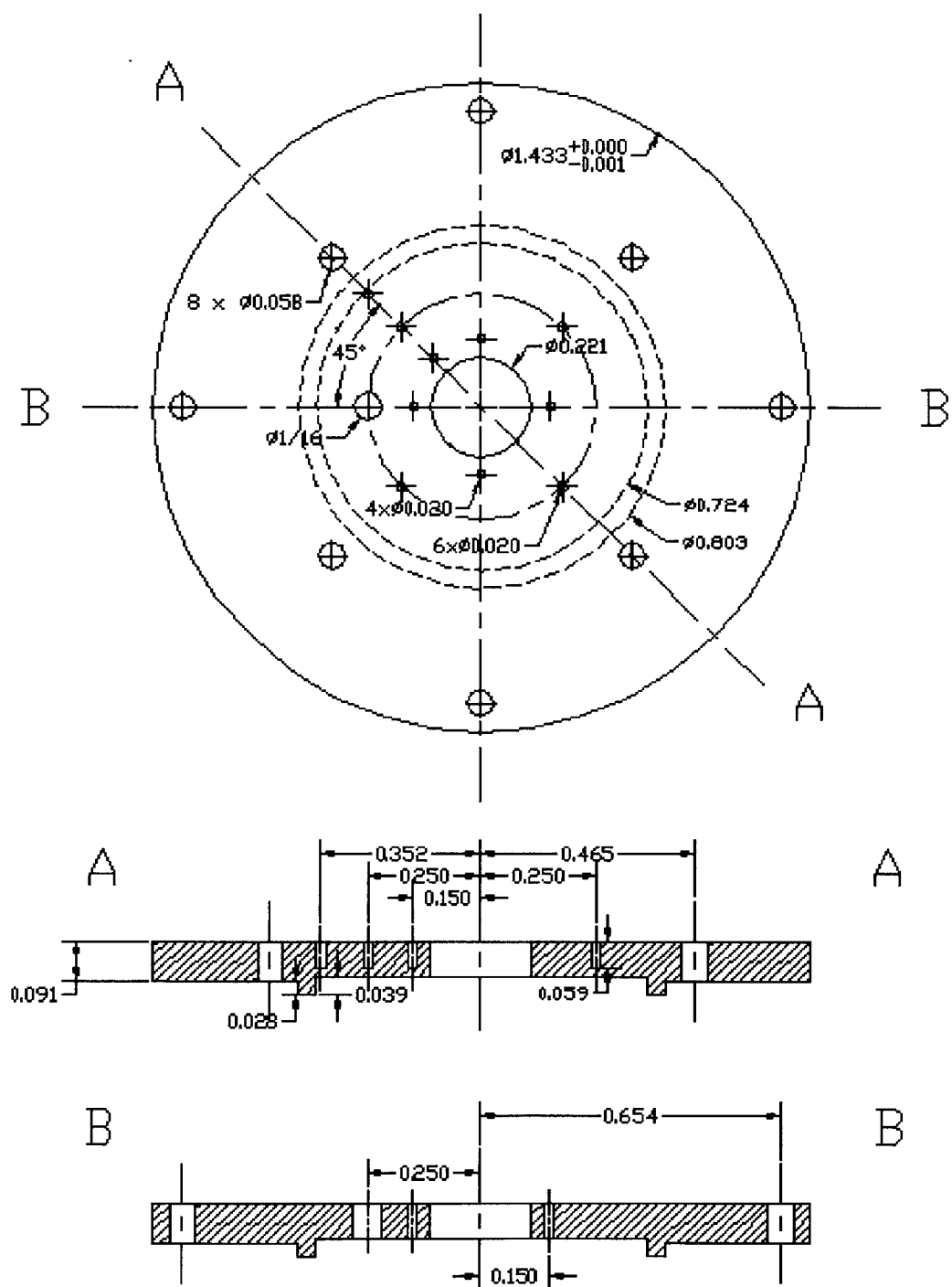


Figure A.3: Mechanical drawing of the bottom-plate of the catalytic flow reactor

BIBLIOGRAPHY

- [1] ABAQUS/Standard User's Manual, Version 6.3, Hibbit, Karlsson & Sorensen, Inc., 2002.
- [2] Epstein et al., "The MIT Microengine Project", Annual Technical Report, 2001.
- [3] Dubrowski, V., personal communication.
- [4] <http://www.goodfellow.com>, Goodfellow Corporation.
- [5] <http://www.usseal.com>, American Seal & Packing, Division of Steadman & Associates, Inc..
- [6] Incropera, F. P. and De Witt, D. P., "Fundamentals of Heat and Mass Transfer", Fifth edition, John Wiley & Sons, 2002.
- [7] Lee, J. W., "Numerical Simulation of a Hydrogen Micro-combustor", S.M. Thesis, Massachusetts Institute of Technology, May 2000.
- [8] Lukachko, S., personal communication.
- [9] Marble, F., personal communication.
- [10] Mehra, A., "Development of a High Power Density Combustion System for a Silicon Micro Gas Turbine Engine", Ph.D. Thesis, Massachusetts Institute of Technology, February 2000.
- [11] Moon, H. S., personal communication.
- [12] Spadaccini et al., "High Power Density Silicon combustion Systems for Micro Gas Turbine Engines", Proceedings of ASME TURBO EXPO 2002, June 2002, GT-2002-30082.
- [13] Spadaccini et al., "Preliminary Development of a Hydrocarbon-fueled Catalytic Micro-combustor", Sensors and Actuators A: Physical, Vol. 103, pp. 219-224, January 2003.
- [14] Spadaccini, C. M., PhD Thesis, Massachusetts Institute of Technology, expected 2003.
- [15] Spearing, M., personal communication.

- [16] Tzeng, Y-S., "An Investigation of Microcombustion Thermal Phenomena", S.M. Thesis, Massachusetts Institute of Technology, 1997.
- [17] Vesper, G. and Schmidt, L.D., "Ignition and Extinction in the Catalytic Oxidation of Hydrocarbons", AIChE Journal, Vol. 42, pp. 1077-1087, 1996.